

<sub>1</sub> Study of neutrino-nucleus interaction at around 1 GeV using  
<sub>2</sub> hollow cuboid lattice neutrino detectors, WAGASCI, muon  
<sub>3</sub> range detectors and magnetized spectrometer, Baby MIND,  
<sub>4</sub> at J-PARC neutrino monitor hall

<sub>5</sub> A. Bonnemaison, R. Cornat, L. Domine, O. Drapier, O. Ferreira, F. Gastaldi,  
<sub>6</sub> M. Gonin, J. Imber, M. Licciardi, F. Magniette, T. Mueller, L. Vignoli, and O. Volcy

<sub>7</sub> *Ecole Polytechnique, IN2P3-CNRS, Laboratoire Leprince-Ringuet, Palaiseau,*  
<sub>8</sub> *France*

<sub>9</sub> S. Cao and T. Kobayashi

<sub>10</sub> *High Energy Accelerator Research Organization (KEK), Tsukuba, Ibaraki, Japan*

<sub>11</sub> M. Khabibullin, A. Khotjantsev, A. Kostin, Y. Kudenko, A. Mefodiev, O. Mineev,  
<sub>12</sub> S. Suvorov, and N. Yershov

<sub>13</sub> *Institute for Nuclear Research of the Russian Academy of Sciences, Moscow, Russia*

<sub>14</sub> B. Quilain

<sub>15</sub> *Kavli Institute for the Physics and Mathematics of the Universe (WPI), The*  
<sub>16</sub> *University of Tokyo Institutes for Advanced Study, University of Tokyo, Kashiwa,*  
<sub>17</sub> *Chiba, Japan*

<sub>18</sub> T. Hayashino, A. Hiramoto, A.K. Ichikawa, K. Nakamura, T. Nakaya, K Yasutome,  
<sub>19</sub> and K. Yoshida

<sub>20</sub> *Kyoto University, Department of Physics, Kyoto, Japan*

<sub>21</sub> Y. Azuma, J. Harada, T. Inoue, K. Kin, N. Kukita, S. Tanaka, Y. Seiya,  
<sub>22</sub> K. Wakamatsu, and K. Yamamoto

<sub>23</sub> *Osaka City University, Department of Physics, Osaka, Japan*

<sup>24</sup> A. Blondel, F. Cadoux, Y. Favere, E. Noah, L. Nicola, and S. Parsa

<sup>25</sup> *University of Geneva, Section de Physique, DPNC, Geneva, Switzerland*

<sup>26</sup> N. Chikuma, F. Hosomi, T. Koga, R. Tamura, and M. Yokoyama

<sup>27</sup> *University of Tokyo, Department of Physics, Tokyo, Japan*

<sup>28</sup> Y. Hayato

<sup>29</sup> *University of Tokyo, Institute for Cosmic Ray Research, Kamioka Observatory,  
30 Kamioka, Japan*

<sup>31</sup> Y. Asada, K. Matsushita, A. Minamino, K. Okamoto, and D. Yamaguchi

<sup>32</sup> *Yokohama National University, Faculty of Engineering, Yokohama, Japan*

<sup>33</sup> December 14, 2017

# **34** Contents

<b>35</b>	<b>1</b>	<b>Introduction</b>	<b>4</b>
<b>36</b>	<b>2</b>	<b>Experimental Setup</b>	<b>4</b>
37	2.1	WAGASCI modules . . . . .	6
38	2.1.1	Detector . . . . .	6
39	2.1.2	Electronics . . . . .	9
40	2.1.3	Water system . . . . .	10
41	2.2	INGRID Proton module . . . . .	10
42	2.3	Baby MIND . . . . .	12
43	2.3.1	Magnet modules . . . . .	12
44	2.3.2	Scintillator modules . . . . .	14
45	2.3.3	Electronics . . . . .	14
46	2.3.4	Pefromance check . . . . .	16
47	2.4	Side muon range detector . . . . .	16
<b>48</b>	<b>3</b>	<b>Physics goals</b>	<b>18</b>
49	3.1	Expected number of events . . . . .	19
50	3.2	Pseudo-monochromatic beam by using different off-axis fluxes . . . . .	19
51	3.3	Extraction of Cross sections . . . . .	21
52	3.4	Subjects WAGASCI can contribute . . . . .	21
<b>53</b>	<b>4</b>	<b>Status of J-PARC T59 experiment</b>	<b>23</b>
<b>54</b>	<b>5</b>	<b>MC studies</b>	<b>24</b>
55	5.1	Simulation setup . . . . .	24
56	5.2	Event selection . . . . .	27
<b>57</b>	<b>6</b>	<b>Standalone WAGASCI-module performances</b>	<b>29</b>
58	6.1	Reconstruction algorithm . . . . .	31
59	6.1.1	Description . . . . .	31
60	6.1.2	Performances . . . . .	33
61	6.2	Background substraction: the water-out module . . . . .	37
<b>62</b>	<b>7</b>	<b>Schedule</b>	<b>40</b>
<b>63</b>	<b>8</b>	<b>Requests</b>	<b>40</b>
64	8.1	Neutrino beam . . . . .	40
65	8.2	Equipment request including power line . . . . .	40

**Abstract**68 **1 Introduction**

69 The understanding of neutrino-nucleus interactions in the 1 GeV energy region is critical  
 70 for the success of accelerator-based neutrino oscillation experiments such as the T2K exper-  
 71 iment. Complicated multi-body effects of nuclei render this understanding difficult. The  
 72 T2K near detectors have been measuring these and significant progress has been achieved.  
 73 However, the understanding is still limited. One of the big factors preventing a complete  
 74 understanding is the non-monochromatic neutrino beam spectrum. Measurements with  
 75 distinct but partially overlapping beam spectra would be a great benefit in resolving the  
 76 contribution from different neutrino energies. We, the WAGASCI collaboration, proposes  
 77 to study the neutrino-nucleus interaction at the B2 floor of the neutrino monitor building,  
 78 where different neutrino spectra from the T2K off-axis near detector (ND280) can be ob-  
 79 tained due to the different off-axis position. Our experimental setup contains two hollow  
 80 cuboid lattice detectors as the neutrino interaction target (known as WAGASCI modules),  
 81 two side- and one downstream- muon range detectors(MRD's). We will have two types of  
 82 the WAGASCI modules, a water-in module and a water-out module. The water-in WA-  
 83 GSCI module has water the hollow cuboid lattice, and the water-out WAGASCI module  
 84 doesn't have water inside the lattice. The hollow cuboid lattice and side-MRD's allow a  
 85 measurement of wider-angle scattering than ND280. High water to scintillator material  
 86 ratio enables the measurement of the neutrino interaction with water, which is highly de-  
 87 sired for the T2K experiment because it's far detector, Super-Kamiokande, is composed of  
 88 water. The MRD's consist of plastic scintillators and iron plates. The downstream-MRD,  
 89 so called the Baby MIND detector, also works as a magnet and provides the charge iden-  
 90 tification capability as well as magnetic momentum measurement for high energy muons.  
 91 The charge identification is essentially important to select antineutrino events in the an-  
 92 tineutrino beam because contamination of the neutrino events is as high as 30%. Most of  
 93 the detectors have already been constructed. The WAGASCI modules have been commis-  
 94 sioned as the J-PARC T59 experiment and the Baby MIND detector was commissioned at  
 95 the CERN neutrino platform. Therefore, the collaboration will be ready to proceed to the  
 96 physics data taking for the T2K beam time in January 2019. We will provide the cross sec-  
 97 tions of the charged current neutrino and antineutrino interactions on water with slightly  
 98 higher neutrino energy than T2K ND280 with wide angler acceptance. When combined  
 99 with ND280 measurements, our measurement would greatly improve the understanding  
 100 of the neutrino interaction at around 1 GeV and contribute to reducing one of the most  
 101 significant uncertainties of the T2K experiment.

102 **2 Experimental Setup**

103 Figure 1 and 2 show a schematic view and a CAD drawing of the entire set of detectors.  
104 Central neutrino target detectors consist of two WAGASCI modules and T2K INGRID  
105 proton module. Inside the WAGASCI module, plastic scintillator bars are aligned as a  
106 hollow cuboid lattice and spaces in the lattice are filled with water for a water-in WAGASCI  
107 module. T2K INGRID proton module is a full active neutrino target detector which is  
108 composed only with scintillator bars in its tracking region. The central detectors are  
109 surrounded by two side- and one downstream- muon range detectors(MRD's) The MRD's  
110 are used to select muon tracks from the charged-current (CC) interactions and to reject  
111 short tracks caused by neutral particles that originate mainly from neutrino interactions in  
112 material surrounding the central detector, like the walls of the detector hall, neutrons and  
113 gammas, or neutral-current (NC) interactions. The muon momentum can be reconstructed  
114 from its range inside the detector. The MRD's consist of plastic scintillators and iron plates.  
115 The downstream-MRD, also known as the Baby MIND detector, additionally has a coil  
116 wound around each of the iron plates so it may be magnetized. This provides the charge  
117 selection capability.

118 For all detectors, scintillation light in the scintillator bar is collected and transported  
119 to a photodetector with a wavelength shifting fiber (WLS fiber). The light is read out by  
120 a photodetector, Multi-Pixel Photon Counter (MPPC), attached to one end of the WLS  
121 fiber. The signal from the MPPC is read out by the dedicated electronics developed for  
122 the test experiment to enable bunch separation in the beam spill. The readout electronics  
123 are triggered using the beam-timing signal from MR to synchronize to the beam. The  
124 beam-timing signal is branched from those for T2K, and will not effect T2K data taking.

125 T2K adopted the off-axis beam method, in which the neutrino beam is intentionally  
126 directed 2.5 degrees away from SK producing a narrow band  $\nu_\mu$  beam. The off-axis near  
127 detector, ND280, is installed towards the SK direction in the B1 floor of the near detector  
128 hall of the J-PARC neutrino beam-line. We propose to install our detector in the B2 floor  
129 of the near detector hall, where the off-axis angle of 1.5 degrees is slightly different to the  
130 2.5 degrees of ND280. The candidate detector position in the B2 floor is shown in Figure  
131 3. The expected neutrino energy spectrum at the candidate position is shown in Figure 4.

132 **2.1 WAGASCI modules**

133 **2.1.1 Detector**

134 The WAGASCI modules are mainly composed of 1280 plastic scintillator bars and a sur-  
135 rounding stainless steel tank as shown in Figure 5. The total number of channels in one  
136 WAGASCI module is 1280. The stainless steel tank is constructed by welding stainless  
137 steel plates, is sized as 460mm×1250mm×1250 mm, and weighs 0.5 tonne.

138 One WAGASCI module consists of 16 scintillator tracking planes, where each plane  
139 is an array of 80 scintillator bars fixed with ABS frames. The 40 bars, called parallel

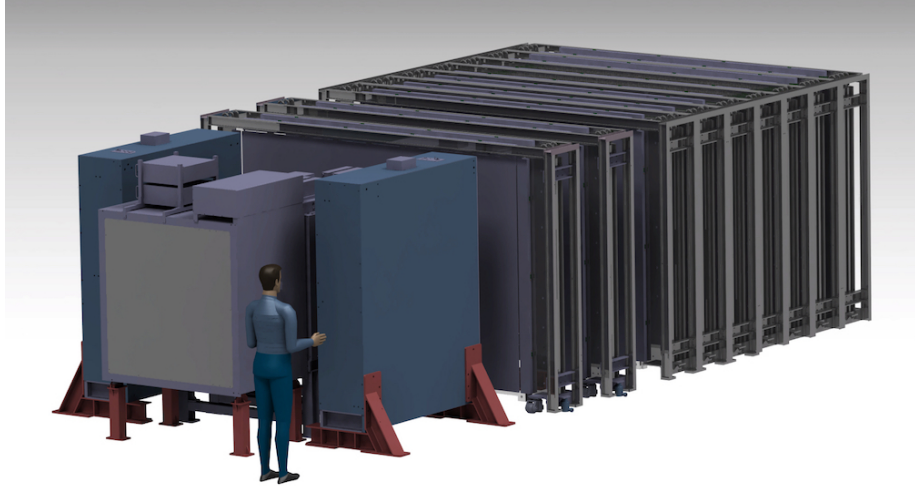


Figure 1: Schematic view of entire sets of detectors.

140 scintillators, are placed perpendicularly to the beam, and the other 40 bars, called lattice  
 141 scintillators, are placed in parallel to the beam with hollow cuboid lattice in the tracking  
 142 plane as shown in Figure 5. Thanks to the hollow cuboid lattice of the scintillator bars,  
 143 the WAGASCI module has  $4\pi$  angular acceptance for charged particles.

144 Thin plastic scintillator bars produced at Fermilab by extrusion method, mainly consists  
 145 of polystyrene and are surrounded by thin reflector including  $\text{TiO}^2$  (3 mm in thickness)  
 146 are used for the WAGASCI modules to reduce the mass ratio of scintillator bars to water,  
 147 because neutrino interactions in the scintillator bars are a background for the cross section  
 148 measurements on  $\text{H}_2\text{O}$ . Each scintillator bar is sized as 1020mm×25mm×3 mm including  
 149 the reflector part, and half of all the scintillator bars have 50-mm-interval slits to form the  
 150 hollow cuboid lattice (Figure 6 ).

151 We will have two types of the WAGASCI modules, a water-in module and a water-out  
 152 module. The water-in WAGASCI module has water in spaces of the hollow cuboid lattice.  
 153 The total water mass serving as neutrino targets in the fiducial volume of the module is  
 154 188 kg, and the mass ratio of scintillator bars to water is 80 %. The water-out WAGASCI  
 155 module doesn't have water inside the detector. The total CH mass serving as neutrino  
 156 target in the fiducial volume of the module is 47 kg, and the mass fraction of scintillator  
 157 bars is 100 %.

158 Scintillation light is collected by wave length shifting fibers, Y-11 (non-S type with a  
 159 diameter of 1.0 mm produced by Kuraray. A fiber is glued by optical cement in a groove  
 160 on surface of a scintillator bar. 32 fibers are gathered together by a fiber bundle at edge  
 161 of the module, and lead scintillation light to a 32-channel arrayed MPPC. Since crosstalk

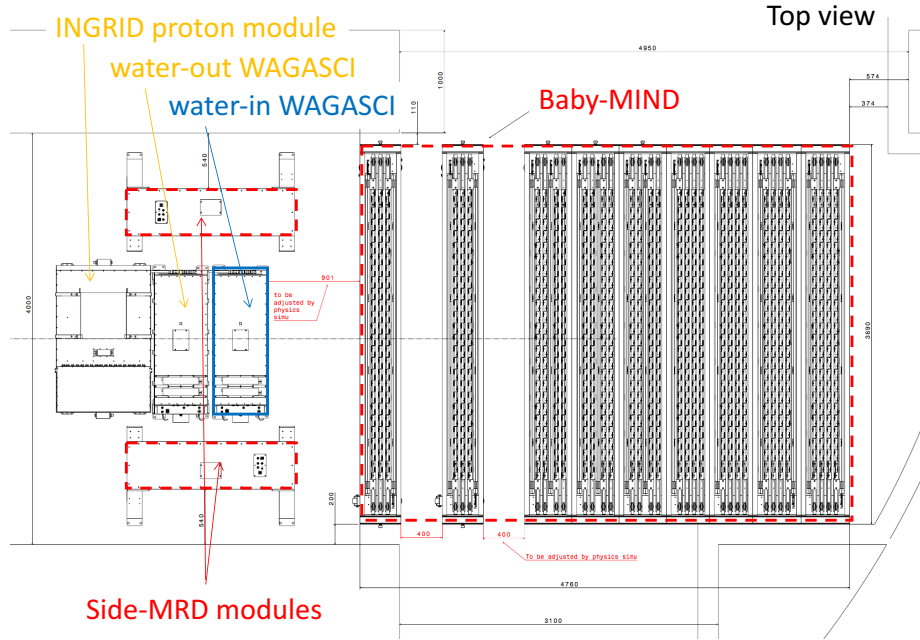


Figure 2: Top view of entire sets of detectors.

of light yield due to reflection on the inner surface of each cell has been observed, all the scintillator bars are painted black by aqueous color spray. It is confirmed by measurements with cosmic rays that black painting on the surface of the scintillator bars suppresses this crosstalk so that no significant crosstalk effect is observed within uncertainty.

32-channel arrayed MPPCs, as shown in the Figure 7, are used for the modules. The surface of the fiber bundle is polished and directly attached onto the 32-channel arrayed MPPCs. The positions of 32 fibers on the bundle are aligned to fit the channels of MPPCs. The MPPC is a product of Hamamatsu Photonics, S13660(ES1), with suppressed noise rate of  $\sim$ 6 kHz per channel at 0.5 p.e. threshold. For each MPPC channel, 716 pixels of APD are aligned in a shape of circle.

172 2.1.2 Electronics

173 As front-end electronics of this detector, a Silicon PM Integrated Read-Out Chip (SPIROC)  
174 [13] is adopted. SPIROC is a 36-channel auto-triggered front-end ASIC, and is produced  
175 by OMEGA/ IN2P3. It not only contains an analog signal processing part such as amplifi-  
176 cation and shaping of the waveform, but contains a digital signal processing parts such as  
177 auto-trigger and timing measurement. Charge of MPPC signal is sampled by track-and-

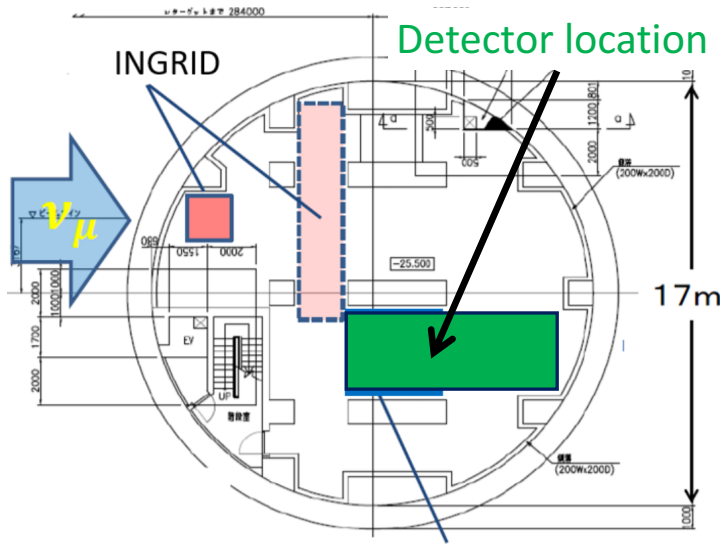


Figure 3: Candidate detector position on the B2 floor of the near detector hall.

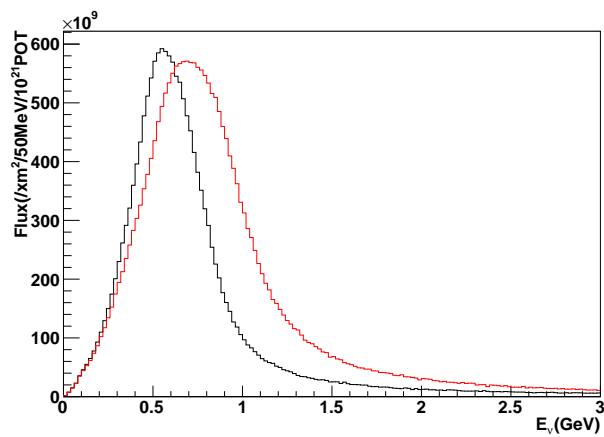


Figure 4: Neutrino energy spectrum at the candidate detector position (red, off-axis 1.5 degree). The spectrum at the ND280 site (black, off-axis 2.5 degree) is also shown.

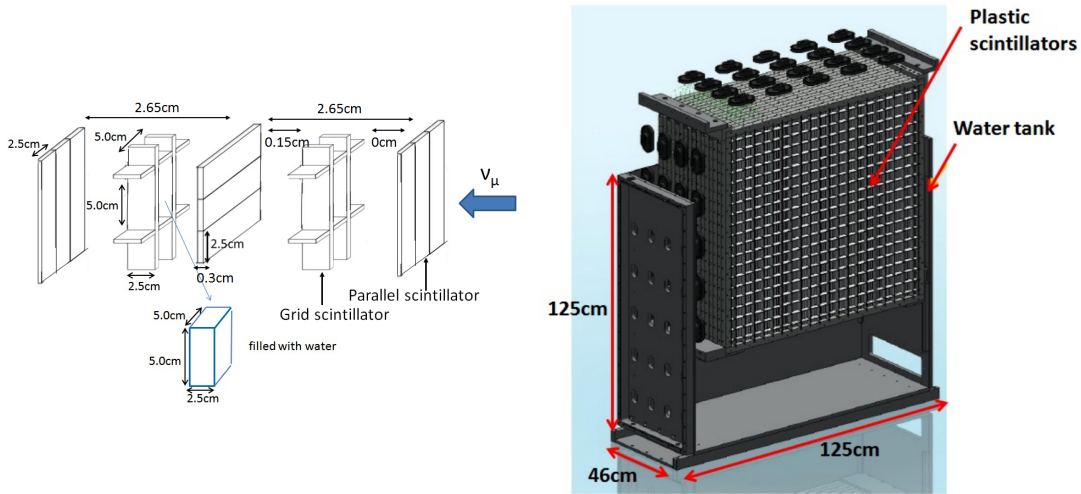


Figure 5: Schematic views of hollow cuboid lattice of plastic scintillator bars (left) and WAGASCI module (right).

hold circuit. A Front-end electronics board, Active Sensor Unit (ASU), has been developed with the SPIROC2D chip, which is the latest version of SPIROC. Each readout board is designed to control a 32-channel arrayed MPPC, and 40 of the ASU boards are aligned on the module surface. The data acquisition system used for this detector, including back-end boards, has been developed for prototypes of ultra-granular calorimeters for the International Linear Collider (ILC) [6], and independent of the T2K DAQ system. To synchronize the DAQ system to J- PARC neutrino beam, pre-beam trigger and beam trigger are sent to the clock control card. The beam trigger signals are converted from optical signals to NIM signals at NIM module on the B2 floor. In addition, the information of spill number are delivered with 16-bit ECL level signals, and converted to an Ethernet frame by an FPGA evaluation board to be directly sent to the DAQ PC. The electronics readout scheme is shown in Figure 8.

### 2.1.3 Water system

Pure water is filled to the water tank of the water-in WAGASCI module as follows. First, the water storage tank located at the B2 floor of the NM pit is filled with water delivered from a water tap on the ground level through a long hose. Second, the water is pumped to the other water storage tank though a water filler to produce pure water. Third, a compound preservative called Germall plus, which is the same preservative used in one of the sub-detectors of T2K ND280, FGD2, is put into the water to keep water from being bad. Then, the water is poured to the water-in WAGASCI module, and it is kept in the

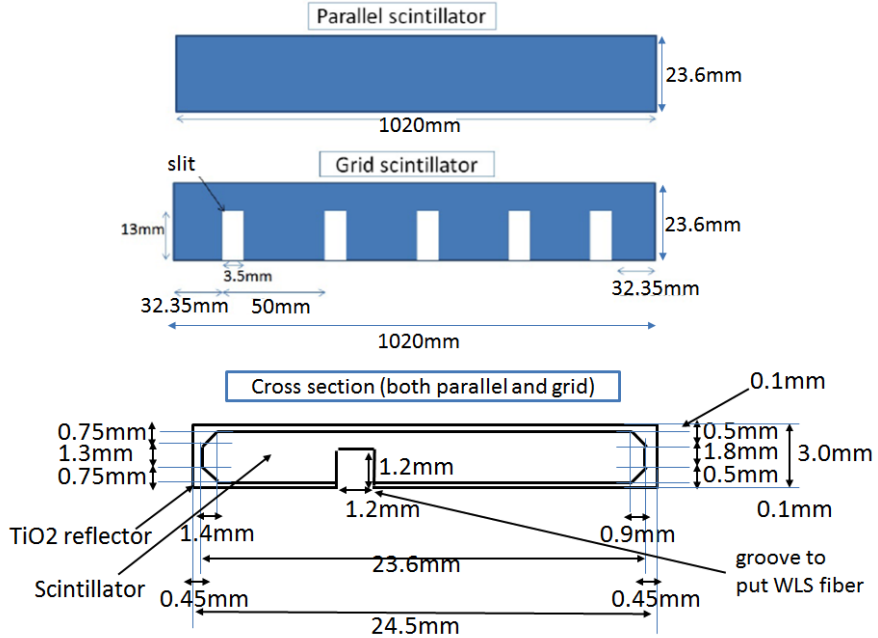


Figure 6: Geometry of scintillators used for WAGASCI modules.

<sup>198</sup> module during the neutrino beam operation and not to be circulated.

## <sup>199</sup> 2.2 INGRID Proton module

<sup>200</sup> INGRID Proton module is a neutrino detector of the T2K experiment. It is a fully-active  
<sup>201</sup> tracking detector which consists of only scintillator strips. The purpose of this Proton  
<sup>202</sup> Module is to separate the neutrino interaction types by detecting the protons and pions  
<sup>203</sup> together with the muons from the neutrino interactions, and to measure the neutrino cross  
<sup>204</sup> section for each interaction type. It consists of 36 tracking planes surrounded by veto  
<sup>205</sup> planes (Figure 9), where each tracking plane is an array of two types of scintillator strips.  
<sup>206</sup> The 16 strips in the inner region have dimensions of  $25\text{mm} \times 13\text{mm} \times 1200\text{mm}$ , while the 16  
<sup>207</sup> strips in the outer region have dimensions of  $50\text{mm} \times 10\text{mm} \times 1200\text{mm}$ , making a plane of  
<sup>208</sup>  $1200\text{mm} \times 1200\text{mm}$  in the horizontal and vertical directions. The former is the scintillator  
<sup>209</sup> produced for the K2K SciBar detector [4] and the latter was produced for INGRID. The  
<sup>210</sup> tracking planes are placed perpendicular to the beam axis at 23mm intervals. Since the  
<sup>211</sup> strips are aligned in one direction, each tracking plane is sensitive to either the horizontal or  
<sup>212</sup> vertical position of the tracks. The tracking planes are therefore placed alternating in the  
<sup>213</sup> horizontal and vertical directions so that three-dimensional tracks can be reconstructed.  
<sup>214</sup> The tracking planes also serve as the neutrino interaction target. As with the WAGASCI

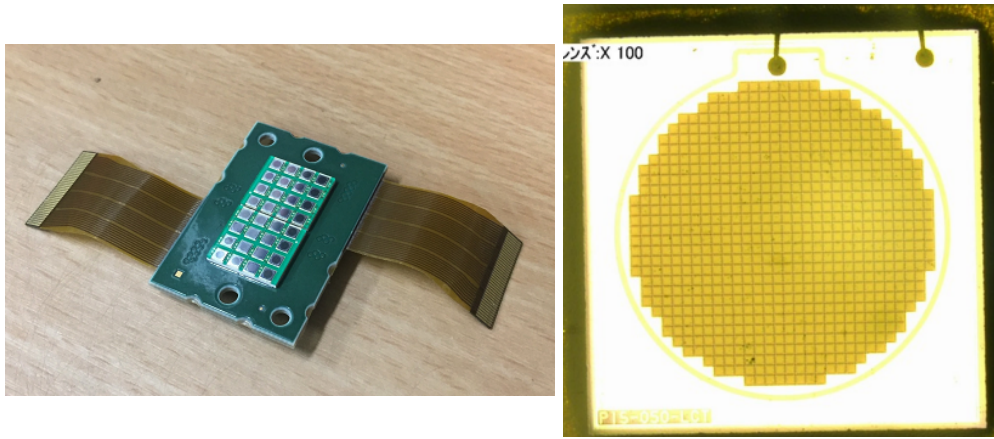


Figure 7: 32-channel arrayed MPPC (left) and an enlarged view of one MPPC channel (right).

215 modules, scintillation light is read out by a WLS fiber and MPPC.

216 It was installed on the neutrino beam axis on the SS floor of the T2K near detector hall  
 217 in 2010, and had been used for neutrino cross section measurements. In August 2017, it  
 218 was moved to the B2 floor of the T2K near detector hall by J-PARC T59 after getting the  
 219 approval from T2K to use them. J-PARC T59 is performing a neutrino beam measurement  
 220 using the detector from October 2017, and the measurement will continue until May 2018  
 221 as we will discuss in Sec. 4.

222 We will operate the INGRID Proton module using the T2K near detector electronics/DAQ  
 223 system in the same way as J-PARC T59. A proposal to use the module and its  
 224 electronics for our project will be submitted to the T2K collaboration.

### 225 2.3 Baby MIND

226 The Baby MIND is the downstream Muon Range Detector. It also works as a magnet and  
 227 provides the charge identification capability as well as magnetic momentum measurement  
 228 for high energy muons.

229 The Baby MIND collaboration<sup>1</sup> submitted a proposal to the SPSC at CERN, SPSC-P-  
 230 353. The project was approved by the CERN research board as Neutrino Platform project  
 231 NP05 and constructed. The detector consists of 33 magnet modules, each 3500 mm ×  
 232 2000 mm × 50 mm (30 mm steel) with a mass of approximately 2 tonnes. Of these magnet  
 233 modules, 18 are instrumented with plastic scintillator modules.

---

<sup>1</sup>Contact person: E. Noah, Spokesperson: A. Blondel, Deputy spokesperson: Y. Kudenko

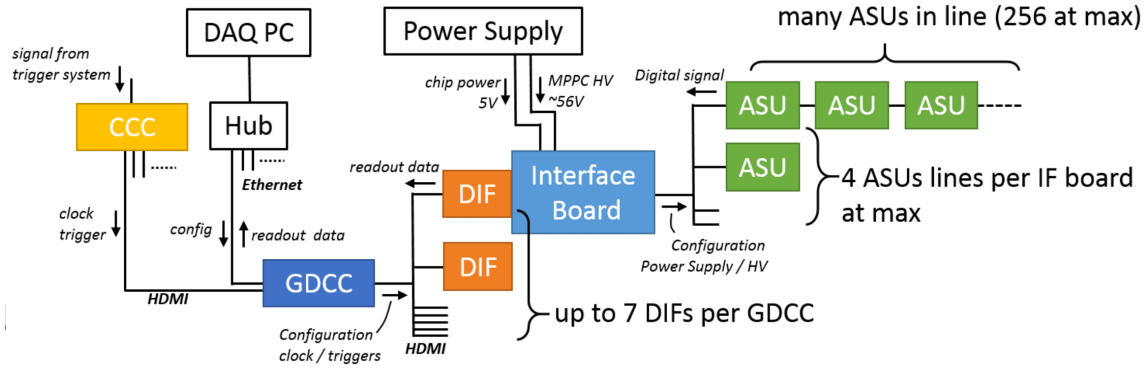


Figure 8: WAGASCI electronics readout scheme.

### 2.3.1 Magnet modules

Traditional layouts for magnetized iron neutrino detectors (e.g. MINOS) tend to be monolithic blocks with a unique pitch between consecutive steel segments and large conductor coils threaded around the whole magnet volume. The Baby MIND detector, like traditional designs, is built from sheets of iron interleaved with scintillator detector modules. However Baby MIND is novel in that the iron segments are all individually magnetized as shown in Figure 10, allowing for far greater flexibility in the setting of the pitch between segments, and in the allowable geometries that these detectors can take.

The key design outcome is a highly optimized magnetic field map. A double-slit configuration for coil winding was adopted to increase the area over which the magnetic flux lines are homogeneous in  $B_x$  across the central tracking region. Simulations show the magnet field map to be very uniform over this central tracking region covering an area of  $2800 \times 2000 \text{ mm}^2$ , Figure 11. The  $B_x$  component dominates in this region, with negligible  $B_y$  and  $B_z$ . This was confirmed by measuring the field with 9 pick-up coils wound around the first module. Subsequent modules were equipped with one pick-up coil. Test results on the 33 modules show all achieve the required field of 1.5 T for a current of 140 A, with a total power consumption of 11.5 kW. The polarity of the field map shown in Figure 11 (middle) can be reversed by changing the power supply configuration.

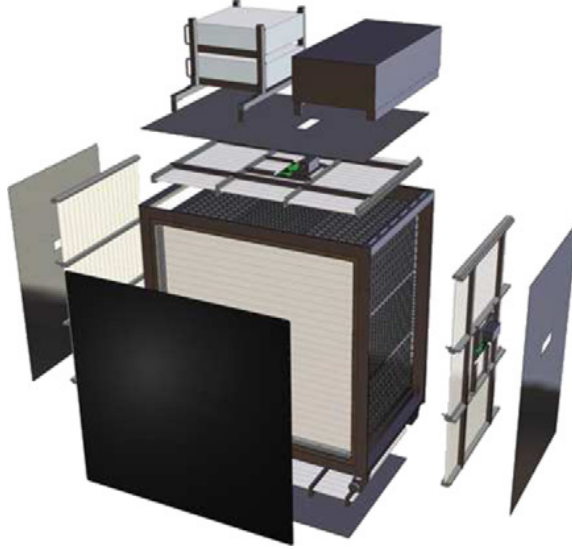


Figure 9: Schematic view of INGRID Proton module.

**2.3.2 Scintillator modules**

Each of the 18 scintillator modules is constructed from 2 planes of horizontal counters (95 counters in total) and 2 planes of vertical counters (16 counters in total) [3], arranged with an overlap between planes to achieve close to 100% hit efficiency for minimum ionizing muons. The arrangement of planes within a module is vertical-horizontal-horizontal-vertical. This arrangement was the result of an assembly approach whereby each plane was built from 2 half-planes, with each half plane consisting of a horizontal plane and a vertical plane. The scintillator bars are held in place using structural ladders that align and maintain the counters, Figure 12. No glue is used in the process, so counters can be replaced. Aluminum sheets front and back provide light tightness.

The plastic scintillator counters were made from 220 mm-wide slabs, consisting of extruded polystyrene doped with 1.5% paraterphenyl (PTP) and 0.01% POPOP. They were cut to size then covered with a 30-100  $\mu\text{m}$  thick diffuse reflector resulting from etching of the surface with a chemical agent [10, 11]. The horizontal counter size is  $2880 \times 31 \times 7.5 \text{ mm}^3$ , with one groove along the length of the bar in which sits a wavelength shifting fiber from Kuraray. The vertical counter size is  $1950 \times 210 \times 7.5 \text{ mm}^3$ , with one U-shaped groove along the bar. On each counter, two custom connectors house silicon photomultipliers, MPPC type S12571-025C from Hamamatsu, either side of the horizontal counter, and both connectors at the top for the vertical counter. This geometrical configuration for vertical counters was chosen for ease of connectivity to the electronics, and maintenance operations.

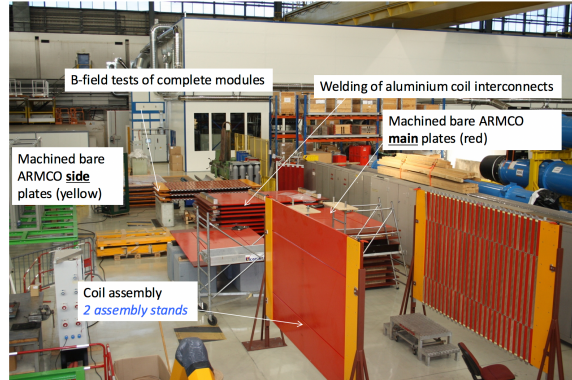


Figure 10: Magnet assembly zone at CERN.

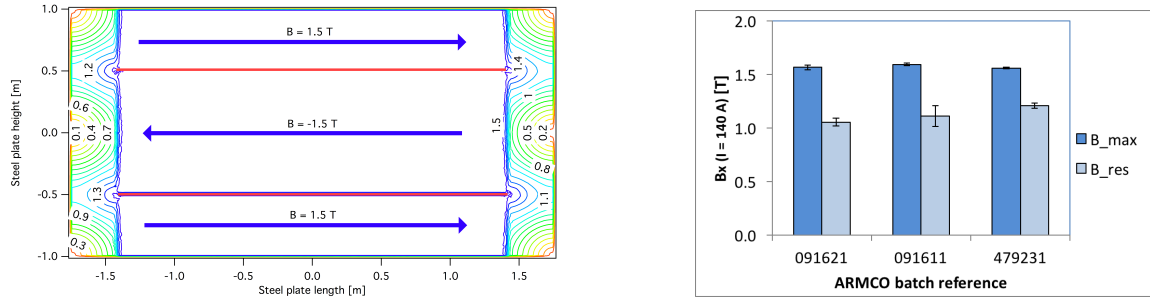


Figure 11: Left) Magnetic field map with a coil along 2800 mm of the length of the plate. Right) Measured B field for 33 modules.



Figure 12: Scintillator modules assembly. Left) top of front half-module showing vertical counters, and the spacer-ladders that set the pitch between horizontal counters and hold them in place. Middle) rear half-module showing horizontal counters on their ladders. Right) Assembled rear half-module, the front half-module can be seen in the background.

273 A total of 1744 horizontal counters and 315 vertical counters (including spares) were  
274 produced at the Uniplast company (Vladimir, Russia).

275 **2.3.3 Electronics**

The Baby MIND electronic readout scheme includes several custom-designed boards [12]. The revised version is shown in Figure 13. At the heart of the system is the electronics Front End Board (FEB), developed by the University of Geneva. The readout system includes two ancillary boards, the Backplane, and the Master Clock Board (MCB) whose development has been managed by INRNE (Bulgarian Academy of Sciences) collaborators.

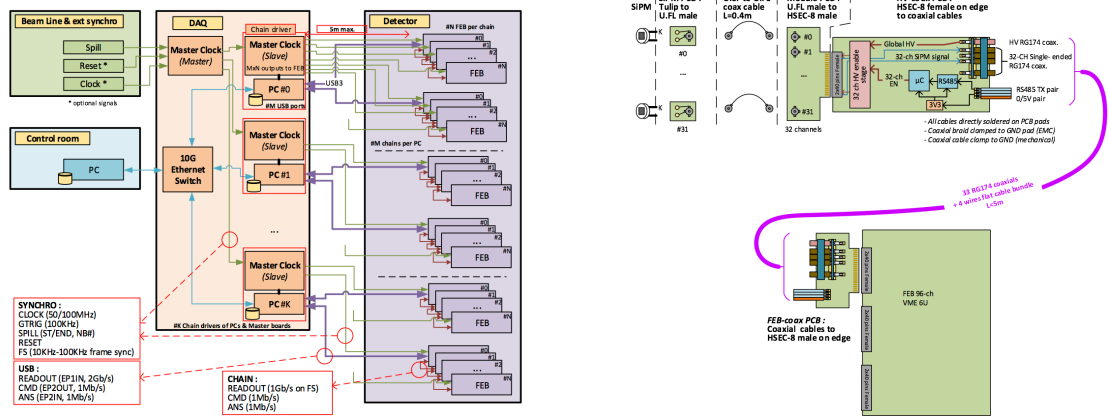


Figure 13: Left) Baby MIND electronics readout scheme. Right) SiPM-to-FEB connectivity.

The FEBv2 hosts 3 CITIROC chips that can each read in signals from 32 SiPMs [7]. Each signal input is processed by a high gain (HG), and a separate low gain (LG), signal path. The outputs from the slow shapers can be sampled using one of two modes: a mode with an externally applied delay, and a peak detector mode. A faster shaper can be switched to either HG or LG paths, followed by discriminators with adjustable thresholds providing 32 individual trigger outputs and one OR32 trigger output. An Altera ARIA5 FPGA on the FEBv2 samples these trigger outputs at 400 MHz, recording rising and falling times for the individual triggers and assigning time stamps to these. Time-over-threshold, the difference between falling and rising times, gives some measure of signal amplitude. This is used in addition to charge information and proves useful if there is more than one hit per bar within the  $\sim 9 \mu\text{s}$  deadtime due to the readout of the multiplexed charge output. The ARIA5 also manages the digitization of the sampled CITIROC multiplexed HG and LG outputs via a 12-bit 8-ch ADC.

294 The internal 400 MHz clock on the FEBv2 can be synchronized to a common 100 MHz  
 295 clock. The synchronization subsystem combines input signals from the beam line into

296 a digital synchronization signal (SYNC) and produces a common detector clock (CLK)  
 297 which can eventually be synchronised to an external experiment clock. Both SYNC and  
 298 CLK signals are distributed to the FEBs. Tests show the FEB-to-FEB CLK(SYNC) delay  
 299 difference to be 50 ps (70 ps). Signals from the beam line at WAGASCI include two  
 300 separate timing signals, arriving 100 ms and 30  $\mu$ s before the neutrino beam at the near  
 301 detectors. The spill number is available as a 16-bit signal.

### 302 2.3.4 Pefromance check

303 All counters were measured at INR Moscow with a cosmic ray setup using the same type  
 304 S12571-025C MPPCs and a CAEN DT5742 digitizer. The average light yield (sum from  
 305 both ends) was measured to be 37.5 photo-electrons (p.e.) per minimum ionizing particle  
 306 (MIP) and 65 p.e./MIP for vertical and horizontal counters, respectively. After shipment  
 307 to CERN, all counters were individually re-tested with an LED [?]. 0.1% of counters  
 308 failed the LED tests and were therefore not used during the assembly of modules. The  
 309 assembly of modules was completed in June 2017, and it was then tested in June and July  
 310 2017 at the Proton Synchrotron experimental hall at CERN with a mixed particle beam  
 311 comprising mostly muons whose momenta could be selected between 0.5 and 5 GeV/c. An  
 event display from the summer 2017 tests is shown in Figure 14.

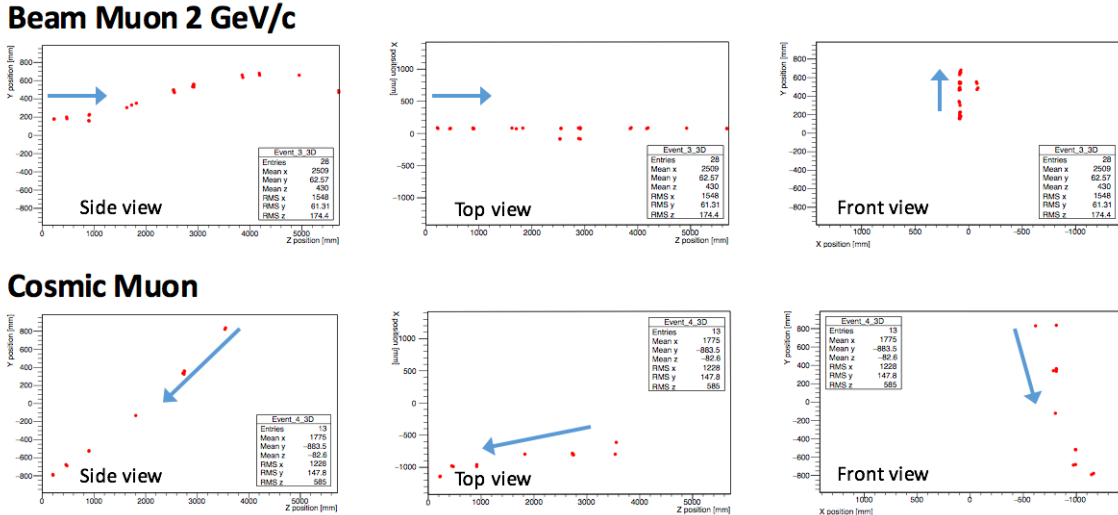


Figure 14: Comparison of a beam muon and cosmic muon in the three different geometrical projections of the detector. The beam impinges on the detector from the left. The arrows indicate the direction of travel of these muons. The direction of the cosmic muon is inferred from timing information.

312

313    **2.4 Side muon range detector**

314    Two Side-MRD modules for tracking secondary particles from neutrino interactions will be  
315    installed in 2018. Each Side-MRD module is composed of 11 steel plates and 80 scintillator  
316    slabs. The slabs are arranged as 10 layers installed in the 13 mm gaps between the 30 mm  
317    thick plates. Each steel plate size is 30 mm  $\times$  1610 mm  $\times$  1800 mm. Total module size is  
318    2236 mm  $\times$  1630 mm  $\times$  975 mm as shown in Figure 15 (left), weight is  $\sim$ 8.5 tonne.

319    Scintillator bars were manufactured by Uniplast company in Vladimir, Russia. Polystyrene  
320    based scintillators were extruded with thickness of 7 mm, then cut to the size of 7  $\times$  200  $\times$   
321    1800 mm<sup>3</sup>. Dopant composition is 1.5% PTP and 0.01% POPOP. Scintillator surface was  
322    etched by a chemical agent to form a white diffuse layer with excellent reflective perfor-  
323    mance. Ideal contact between the scintillator and the reflector raises the light yield up  
324    to 50% comparing to an uncovered scintillator. A sinusoidal groove was milled along the  
325    scintillator to provide uniform light collection over the whole scintillator surface. WLS Y11  
326    Kuraray fiber of 1 mm diameter was glued with an optical cement EJ-500 in the S-shape  
327    groove as shown in Figure 15(right). A minimum bending radius of 30 mm was used to  
328    ensure the the Kuraray S-type fibers remained within specification. Both ends of the fiber  
329    were glued into optical connectors which were themselves attached to the scintillator and  
330    provide an interface to SiPMs, Hamamatsu MPPC S13081-050CS(X1).

331    Scintillators for the Side-MRD modules were assembled at INR in Russia, and shipped  
332    to Japan in July 2017. The light yield for each scintillator was measured with cosmic  
333    rays at INR and at YNU in Japan after delivery.  $LY_1$  and  $LY_2$  are light yields measured  
334    at both ends of the counter. The light yield asymmetry between the ends calculated as  
335     $100\% \times \frac{LY_1 - LY_2}{LY_1 + LY_2}$ . After tests at INR we selected 324 counters from measured 332 ones with  
336    the mean light yield of 45 p.e./MIP ( $LY_1 + LY_2$ ) and the asymmetry value less than 10  
337    %. The measurements at YNU yielded the average total light yield of about 40 p.e./MIP  
338    which varies in range from 32 to 50 p.e./MIP (Figure 16 (left)). Only two counters showed  
339    relatively high asymmetry close to 25 % as shown in Figure 16 (right). Using the results of  
340    the quality assurance test we selected 320 scintillator counters for the Side-MRD modules.

341    We also measured the time resolution for a combination of four counters piled one  
342    upon another. The average result for four counters is  $\sigma_T = 1.04$  ns. The resolution of  
343    combination of 2, 3, 4 counters is measured to be 0.79 ns, 0.66 ns and 0.58 ns, respectively.

344  
345    Construction of the Side-MRD modules is scheduled from November 2017 at Yokohama  
346    National University. They will then be transported to J-PARC for installation on the B2  
347    floor of the T2K near detector hall.

348    Same electronics as the WAGASCI modules (see Sec. 2.1.2) are used for the Side-MRD  
349    modules.

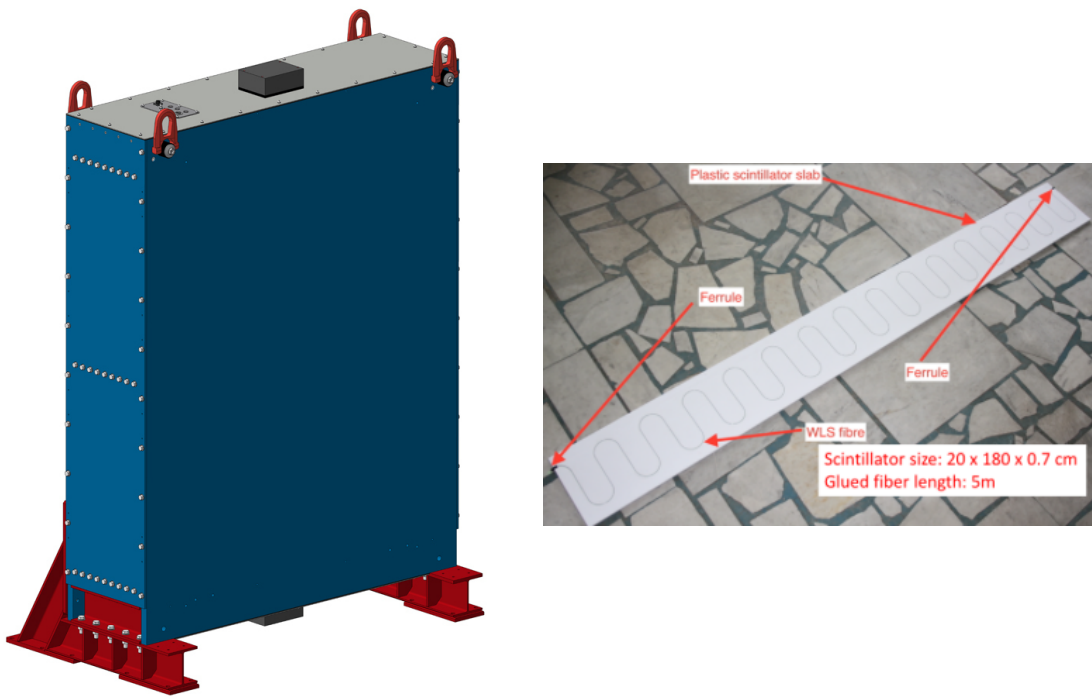


Figure 15: Left :Side-MRD module. Right: Scintillator bar of the Side-MRD modules.

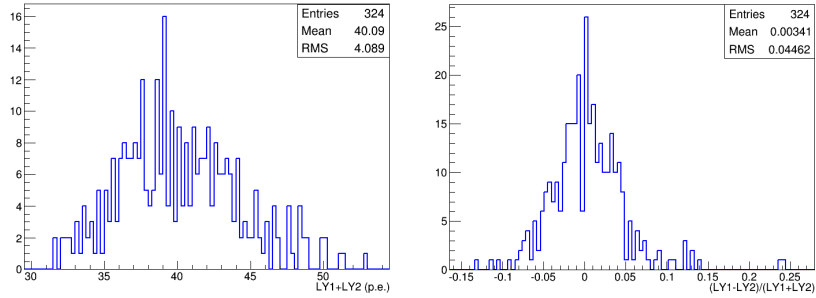


Figure 16: Total light yield distribution (left) and light yield assymetry (right) measured at YNU.

### 3 Physics goals

We will measure the differential cross section for the charged-current (CC) interaction on H<sub>2</sub>O and Hydrocarbon(CH)). The water-scintillator mass ratio of the WAGASCI module is as high as 4:1 and the high purity measurement of the cross section on H<sub>2</sub>O is possible. One experimental option is to remove water from one of the two WAGASCI modules. The water-out WAGASCI module will allow to measure pure-CH target interactions with very low momentum-threshold for protons. This will also allow this CH interaction background to be subtracted from the water-in target measurement. Another option is to add the T2K proton module which is fully made of plastic scintillators. It will allow the high statistics comparison of cross section between H<sub>2</sub>O and CH and also comparison with the ND280 measurement. The actual configuration will be optimized with detailed MC simulation by 2018 Summer.

Our setup allows the measurements of inclusive and also exclusive channels such as 1 $\mu$ , 1 $\mu$ 1p, 1 $\mu$ 1 $\pi^{\pm}$ np samples, the first two of which are mainly caused by the quasi-elastic and 2p2h interaction and the latter is mainly caused by resonant or coherent pion production and deep elastic scattering. In general, an accelerator produced neutrino beam spectrum is wide and the energy reconstruction depends upon the neutrino interaction model. Therefore, recent neutrino cross section measurements including those from T2K are given as a flux-integrated cross section rather than cross sections as a function of the neutrino energy to avoid the model dependency. We can provide the flux-integrated cross section. In addition, by combining our measurements with those from ND280, model-independent extraction of the cross section for narrow energy spread becomes possible. This method was demonstrated in [1] and also proposed by E61 (NUPRISM) experiment.

373 **3.1 Expected number of events**

374 Expected number of CC neutrino events remaining after the event selections was evaluated  
375 with simulation. Details are described in Sec. 5. In neutrino-mode, 5,400, 1,100 and 3,800  
376 events are expected for the water-in WAGASCI module, the water-out WAGASCI module  
377 and the INGRID proton module with  $5 \times 10^{20}$  POT. Among 5,400 events for the water-in  
378 WAGASCI module, 78 % are interactions on H<sub>2</sub>O. In the antineutrino-mode, 2,240, 400  
379 and 1,500 CC antineutrino events are expected for the water-in WAGASCI module, the  
380 water-out WAGASCI module and the INGRID proton module with  $5 \times 10^{20}$  POT. Among 2,  
381 2,240, 74 % are interactions on H<sub>2</sub>O. The wrong-sign interactions in antineutrino-mode is  
382 561 events, but will be removed with 90 % or higher efficiency by Baby MIND.

383 **3.2 Pseudo-monochromatic beam by using different off-axis fluxes**

384 The off-axis method gives narrower neutrino spectrum, and the peak energy is lower for  
385 larger off-axis angle. There still remains a high energy tail mainly due to neutrinos from  
386 Kaon decay. The off-axis angle of the WAGASCI location is 1.5 degrees as opposed to  
387 2.5 degrees for ND280. Top two plots of Figure 17 show the energy spectra of fluxes and  
388 neutrino interaction events at these two different locations. Bottom two plots of Figure 17  
389 show the energy spectra of fluxes and neutrino interaction events obtained by subtraction  
390 of fluxes at ND280 and WAGASCI. We can effectively get two fluxes, from 0.2 GeV to  
391 0.9 GeV and 0.6 GeV and 2 GeV and measure flux-integrated cross section for these two  
392 fluxes. It should be noted that even though the statistical errors are drawn for each energy  
393 bin for the bottom right plot of Fig. 17, measurement results will be given as an integration  
394 across energies.

395 **3.3 Extraction of Cross sections**

The flux-integrated CC inclusive cross sections on H<sub>2</sub>O and CH are calculated from the  
number of selected events with background subtraction and efficiency correction

$$\sigma_{CC} = \frac{N_{sel} - N_{BG}}{\phi T \epsilon},$$

396 where  $N_{sel}$  is the number of selected events from the real data,  $N_{BG}$  is the number of  
397 contaminated background events,  $\phi$  is the integrated  $\nu_\mu$  flux,  $T$  is the number of target  
398 nucleons, and  $\epsilon$  is the detection efficiency for signal estimated by MC simulation. The  
399 number of main background events is effectively estimated from side-band samples. The  
400 CH interaction background for the H<sub>2</sub>O measurement is estimated from the measurement  
401 of the Water-out WAGASCI module and/or the proton module. The neutrino interaction  
402 background for the antineutrino measurement is estimated from the opposite-sign inter-  
403 actions selected by Baby MIND. The dominant error for the inclusive total cross section  
404 measurement is the uncertainty of the neutrino flux, which is ~9% now and is expected

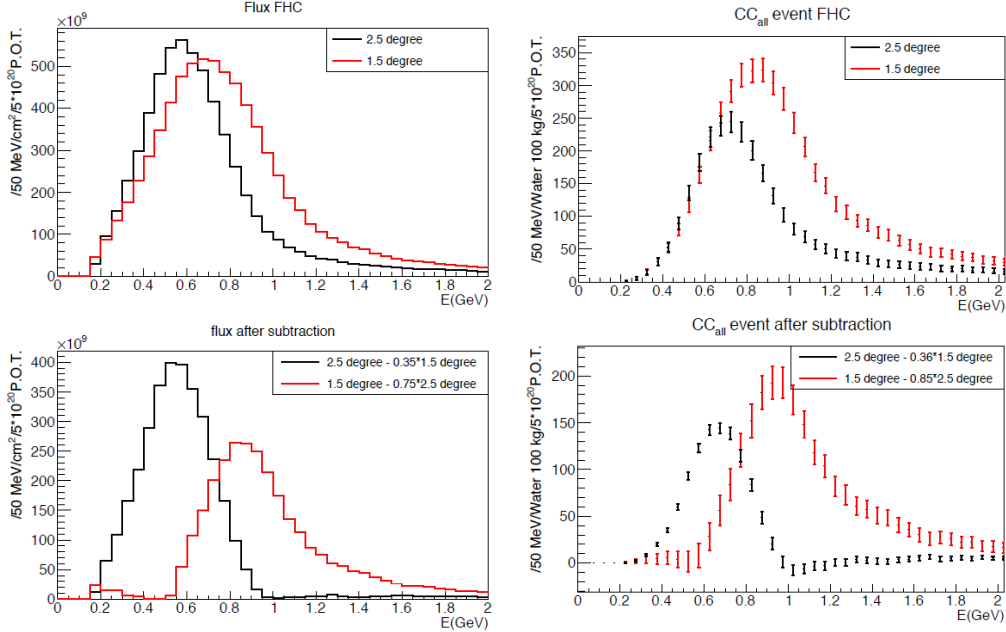


Figure 17: Energy spectra obtained by using different off-axis angle fluxes. Top two plots show the fluxes(left) and spectra of interaction events (right) for ND280 (off-axis 2.5 degree) and WAGASCI (off-axis 1.5 degree). Bottom two plots show the fluxes (left) and spectra of interaction events (right) obtained by subtraction of fluxes at ND280 and WAGASCI. The error bars represent the statistical error and those in the bottom right plot assume the statistical error for ND280 measurements are much smaller than those of the WAGASCI experiment.

405 to be reduced to  $\sim 6\%$ . Since the flux error is dominated by the normalization type error,  
406 the flux error can be significantly reduced for the relative comparison of the H<sub>2</sub>O and CH  
407 cross sections and the relative comparison of the ND280 and WAGASCI measurements.  
408 For example, T2K INGRID succeeded to determine the cross section ratio for CH and  
409 Fe with 3% precision[5]. For the exclusive and/or differential corss section measurements,  
410 statistical error would be dominant, size of which depending on the binning.

411 **3.4 Subjects WAGASCI can contribute**

412 Recent accelerator neutrino experiments use nuclear target e.g. organic scintillator, water  
413 and iron. So the interaction is largely affected by nuclear effects such as Fermi motion,  
414 correlated pairs of nucleons in nucleus (two particles-two holes, 2p2h), collective nuclear  
415 effects and final state interactions (FSI) of secondary particles in the nuclei after the initial  
416 neutrino interactions.

417 The main interaction type at the T2K energy (sub GeV) is the CC quasi-elastic (CCQE)  
418 interaction with nucleons inside nucleus. The energy is reconstructed from the lepton  
419 momentum assuming CCQE kinematics in T2K and other interactions would bias the  
420 reconstructed energy. Figure 18 shows how the reconstructed energy is affected. The 2p2h  
421 interactions mainly happen through the interaction with a correlated nucleons pair and also  
422 through the  $\Delta$  resonance interaction followed by pion-less decay. The 2p2h interactions  
423 are observed in electron scattering experiments [8] where the 2p2h events were observed  
424 in the gap between quasi-elastic region and pion-production region. Neutrino experiments  
425 have attempted to measure the 2p2h interactions, but so far there are only indicative  
426 results because the energy spectrum of the neutrino beam is wide and the precision of the  
427 event-by-event determination of the neutrino energy is not good nor suffered from bias. Our  
428 measurements, when combined with ND280 measurement, will give the cross section values  
429 for narrow energy-spread fluxes and give insight for such interactions. Another efficient  
430 way to investigate the 2p2h interaction is direct measurement of proton tracks with low  
431 momentum threshold and wide acceptance. Figure 19 left plot shows proton multiplicities  
432 for the CCQE events and 2p2h events. Figure 19 right plot shows opening angles of two  
433 proton-tracks for the events having two protons. The water-out WAGASCI can provide  
434 good sample for the 2p2h interaction search because its low density medium enables the  
435 detection of low momentum protons in side acceptance.

436 There are various models which describe the collective nuclear effects [9]. The wide  
437 acceptance of the WAGASCI experiment will provide information complementary to ND280  
438 and will play important role to select and tune models.

439 T2K is starting to use  $\nu_e$  CC1 $\pi$  samples at the far detector to increase the statistics.  
440 One of the biggest uncertainty of the CC1 $\pi$  sample comes from the final state interac-  
441 tions of pions in the nuclei after the initial neutrino interactions because they change the  
442 multiplicity, charge and kinematics of the pions. The multi-pion production events can  
443 be migrated into the CC1 $\pi$  sample due to the FSIs, and they become backgrounds. The

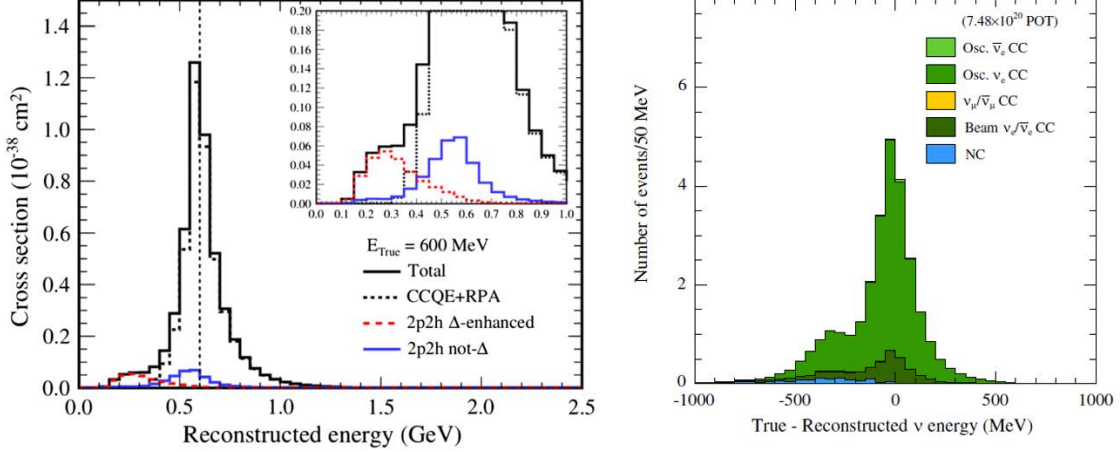


Figure 18: Left: reconstructed neutrino energy for CCQE and 2p2h interactions of 600 MeV muon neutrinos on  $^{12}C$  simulated with a mode. Right: difference between true and reconstructed energy of the  $\nu_e$  CCQE-like sample. The energy is reconstructed from the lepton momentum assuming the kinematics of the CCQE interaction. Both plots from [2]

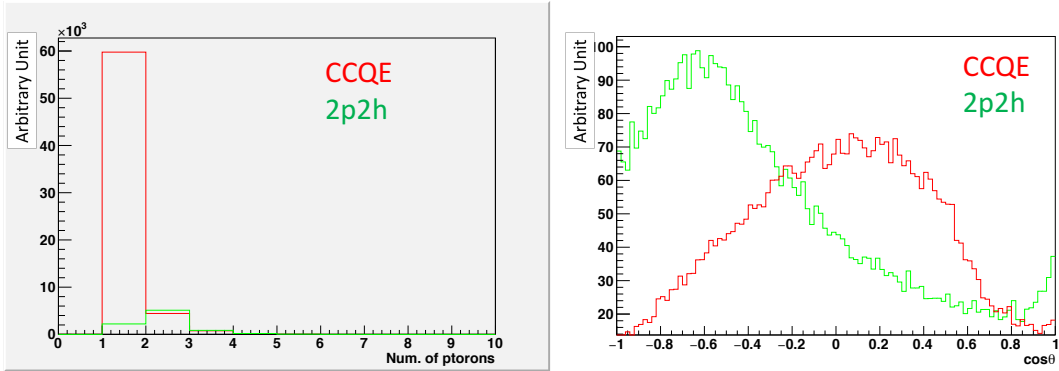


Figure 19: Proton multiplicities (left) and opening angles between two proton tracks (right) for CCQE events and 2p2h events. The final-state interaction is taking into account.

444 WAGASCI module has a capability to distinguish the pion track and proton track from  
445  $dE/dx$ , so WAGASCI can provide the CC $1\pi$  cross section with low momentum threshold  
446 and wide acceptance for pion tracks.

## 447 4 Status of J-PARC T59 experiment

448 We had submitted a proposal of a test experiment to J-PARC in April 2014 to test a new  
449 detector with a water target, WAGASCI, at the neutrino monitor hall, and the proposal  
450 was approved as J-PARC T59. The project contains the side and downstream muon range  
451 detectors as well.

452 The first WAGASCI module has been constructed in 2016 and installed at the on-axis  
453 position in front of the T2K INGRID detector for the commissioning and the first cross  
454 section measurement as a part of the T2K experiment. The INGRID electronics boards are  
455 used to read the signal. The light yield measured with muons produced by the interaction  
456 of neutrinos in the hall wall, shown in Figure 20, is sufficiently high to get a good hit  
efficiency. A track search algorithm based on the cellular automaton has been developed

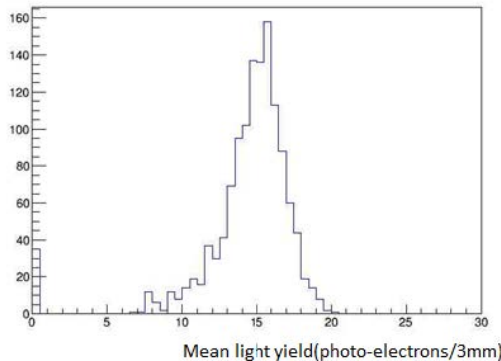


Figure 20: Light yield for muons produced by the interaction of neutrinos in the hall wall.  
Average light yields for each channel are plotted.

457  
458 using the software tools from T2K INGRID. Examples of observed events are shown in  
459 Figure 21. The tracking efficiency in a 2-dimensional projected plane was evaluated by  
460 comparing the reconstructed track in the WAGASCI module and the INGRID module,  
461 and is shown in Figure 22. Note that that the tracking efficiency for high angle ( $> 70$  deg)  
462 is not evaluated because of the acceptance of the INGRID module, not because of the  
463 limitation of the WAGASCI module.

464 In 2017 Autumn, the construction of the second WAGASCI module and the dedicated  
465 electronics board were completed. The module and the electronics were install on the B2

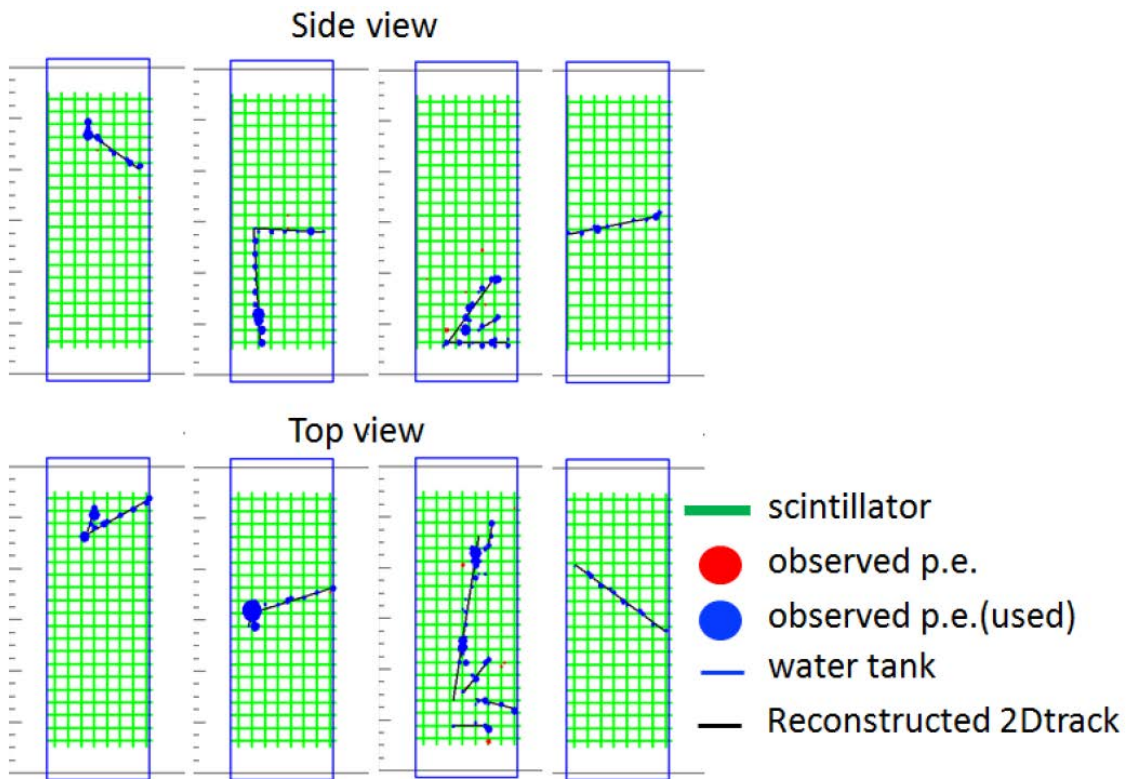


Figure 21: Example event displays of the WAGASCI module at on-axis. The reconstructed tracks are overlaid.

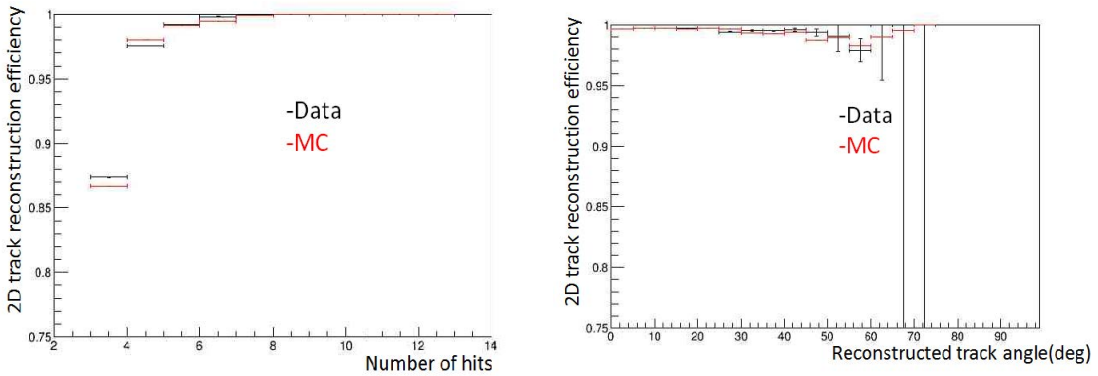


Figure 22: 2D track reconstruction efficiency as a function of number of hits (left) and track angle (right). Here the track angle is the one reconstructed by the INGRID module.

466 floor together with the T2K proton module and the INGRID module as shown in Figure 23.  
 467 The proton module is to be used as the entering muon veto and also for the comparison  
 468 of interaction between CH and Water. The INGRID module will act as the muon detector  
 469 for this period but due to its limited acceptance angle this is only a temporary measure.  
 470 The detector was commissioned and since October has been in operation taking data with  
 471 the T2K antineutrino beam.

472 The production of the components of the side muon range detectors has been completed  
 473 and now the detectors are being assembled at the Yokohama National University. These  
 474 detectors will be installed between January and June 2018, when T2K is not running.

475 The Baby MIND detector was transported from CERN to Japan in December, 2017.  
 476 It will be installed and commissioned in Jan.-Feb. 2018 and T59 will take the neutrino-  
 477 induced muon data in April and May.

## 478 5 MC studies

### 479 5.1 Simulation setup

480 The expected number of neutrino events in the water-in Wagasci detector is predicted by  
 481 Monte Carlo simulations. Neutrino beam flux at the detector location is simulated by  
 482 T2K neutrino flux generator, JNUBEAM. Neutrino interactions with target materials are  
 483 simulated by a neutrino interaction simulator, NEUT. Detector responses are simulated  
 484 using GEANT4-based simulation.

485 The detector geometry in the simulation so far is different from the actual setup as  
 486 shown in Figure 24. The active neutrino target region consists of four WAGASCI modules.

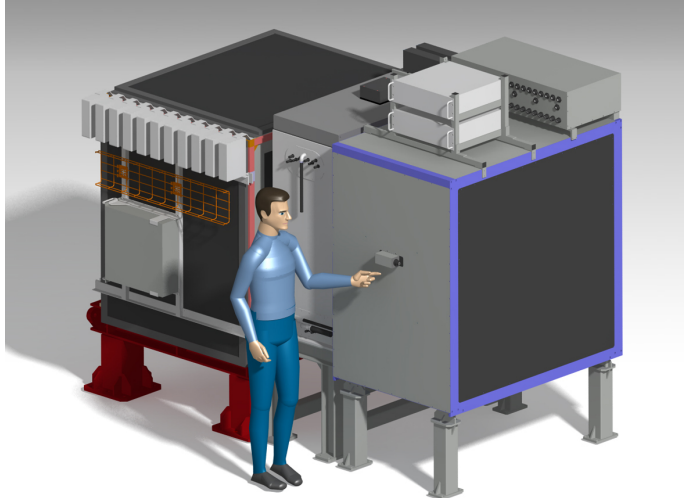


Figure 23: J-PARC T59 detector configuration in October 2017.

487 The size of the WAGASCI module is same as the actual one: 1000 mm  $\times$  1000 mm in the  
 488 x and y directions and 500 mm along the beam direction (z-direction). Two Side-MRD  
 489 modules are installed either side of the Wagasci modules. Each Side-MRD module consists  
 490 of ten iron plates whose dimension is 30 mm (thickness)  $\times$  2000 mm (height)  $\times$  3200 mm  
 491 (width). The distance between the Side-MRD modules and WAGASCI modules is 800  
 492 mm. The downstream-MRD is equivalent to the Baby-MIND, but without the magnetic  
 493 field. It consists of thirty iron plates whose dimension is 30 mm (thickness)  $\times$  2000 mm  
 494 (height)  $\times$  4000 mm (width). The distance between the downstream-MRD modules and  
 495 WAGASCI modules is 800 mm. Update of the study with the actual geometry is now  
 496 underway.

497 To simulate the signal, the energy deposit inside the scintillator is converted into the  
 498 number of photons. The effects of collection and attenuation of the light in the scintillator  
 499 and the WLS fiber are simulated, and the MPPC response is also taken into account. The  
 500 light yield is smeared according to statistical fluctuations and electrical noise.

## 501 5.2 Event selection

502 Tracks are reconstructed in two-dimensional planes in each sub-detector. Then, track  
 503 matching among the sub-detectors and three-dimensional track reconstruction are per-  
 504 formed. These analysis tools have been developed from the software tools by the T2K  
 505 INGRID and in mature stage already.

506 The events are selected as follows. The starting point of the track is required to be

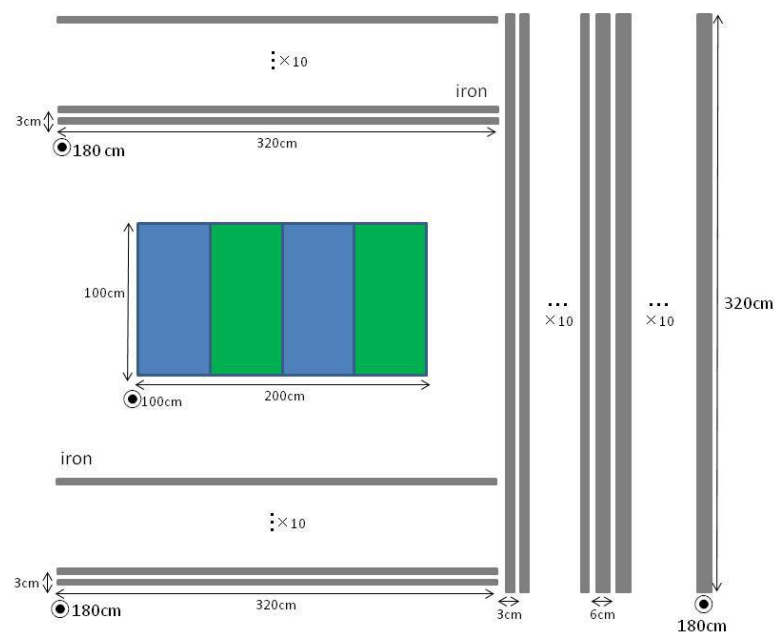


Figure 24: Geometry of the detectors in the Monte Carlo simulation.

507 50 mm away from the edge of the WAGASCI module. This is to remove the background  
 508 from the outside. The longest track has to penetrate more than one (five) iron plates in  
 509 Side-MRD modules (Baby-MIND). This cut select a muon track and rejects backgrounds  
 510 from NC and neutral particles. Then, in order to determine the muon momentum, it is  
 511 required that the longest track stops in MRDs (Side-MRD modules and Baby-MIND) or  
 512 penetrate all iron plates.

513 Table 1 shows numbers of the selected events in one water-in WAGASCI module after  
 514 the event selection. We expect 4,239 (1,666) events from charged-current interaction on  
 515  $H_2O$  with  $5 \times 10^{20}$  POT in (anti)neutrino-mode with one water-in WAGASCI module.  
 516 The purity, when interactions on CH is counted as background, is 78% for the neutrino-  
 517 mode. There is a significant contamination from the wrong-sign (neutrino) interaction for  
 518 antineutrino-mode, however, we expect that it will be removed with efficiency higher than  
 90% by Baby MIND.

Table 1: Expected number of the selected neutrino-candidate events in one water-in WAGASCI module with  $5 \times 10^{20}$  POT in each of neutrino-mode and antineutrino-mode. Note that the wrong sign component will be reduced by one order by applying the charge selection by Baby MIND.

	CC on $H_2O$	NC on $H_2O$	Interaction on CH	wrong sign interaction
$\nu$ -mode	4239	107	1087	(negligible)
anti- $\nu$ -mode	1666	14	560	(561)

519  
 520 Table 2 and 3 summarize contributions classified by the interaction types and final state  
 topologies for the selected charged current-interaction events, respectively.

Table 2: Interaction types for the selected charged-current events.

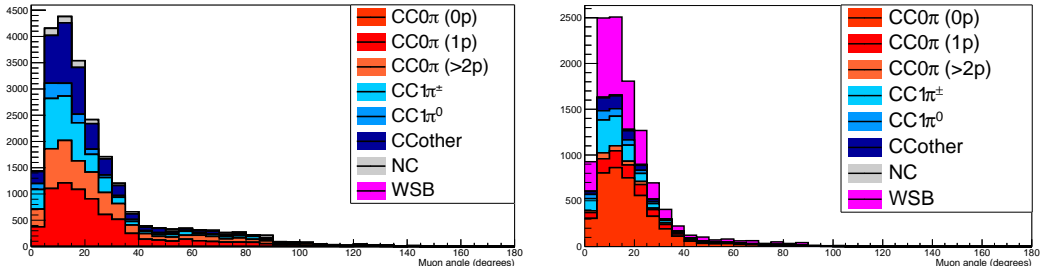
	CCQE	2p2h	CC resonant $\pi$	CC-DIS
$\nu$ -mode	48.4 %	9.7 %	27.1 %	14.7 %
anti- $\nu$ -mode	57.1 %	8.2 %	17.3 %	17.3 %

Table 3: Final state topologies for the selected charged-current events.

	CC0 $\pi$	CC1 $\pi$	CC2 $\pi$	CCn $\pi$
$\nu$ -mode	67.4 %	20.9 %	3.0 %	8.7 %
anti- $\nu$ -mode	79.5 %	16.3 %	1.2 %	3.0 %

521

522     Figure 25 shows the reconstructed angles of the longest tracks in the selected events in  
 523 the neutrino-mode and the anti-neutrino mode. Figure ?? shows the iron plane numbers  
 524 in Side-MRD and Baby-MIND corresponding to the end points of the longest tracks in the  
 selected events in the neutrino-mode and the anti-neutrino mode.



525     Figure 25: The reconstructed angles of the longest tracks in the selected events in the  
 neutrino-mode (left) and the antineutrino-mode (right).

526

## 6 Standalone WAGASCI-module performances

527     In the previous sections, the WAGASCI detector was studied using the Muon Range Detectors.  
 528     In this section, the standalone abilities of WAGASCI module are presented. Using  
 529 the WAGASCI configuration presented in Section 5, we have evaluated that only 7% of  
 530 the muons will be stopped in one of the WAGASCI modules. However, this proportion  
 531 increases to 53% for pions and 73% for protons produced by neutrino interactions at  $1.5^\circ$   
 532 off-axis. Figure 27 shows the momentum distribution of these daughter particles as well as  
 533 for the sub-sample stopped in one of the WAGASCI modules. Therefore, the study of the  
 534 standalone abilities of the WAGASCI module in this section are dominantly motivated by:

- 535     • the accurate measurement of the neutrino interaction final states. Though most of  
 536 the muons will be reconstructed and identified in the MRDs, the hadronic particles  
 537 will predominantly stop in one of the WAGASCI modules. One has therefore to rely  
 538 exclusively on the WAGASCI module information alone to reconstruct, identify and  
 539 measure the momentum of pions or protons.
- 540     • the coverage of the MRDs is not  $4\pi$ . Using the WAGASCI module information can  
 541 therefore help to constrain the particles that exit the WAGASCI module but do not  
 542 enter any MRD.
- 543     • the particle identification of low momenta muons  $p_\mu < 300$  MeV/c that will leave  
 544 only a few hits in the MRD. Using the WAGASCI module information will clearly  
 545 enhance the particle identification.

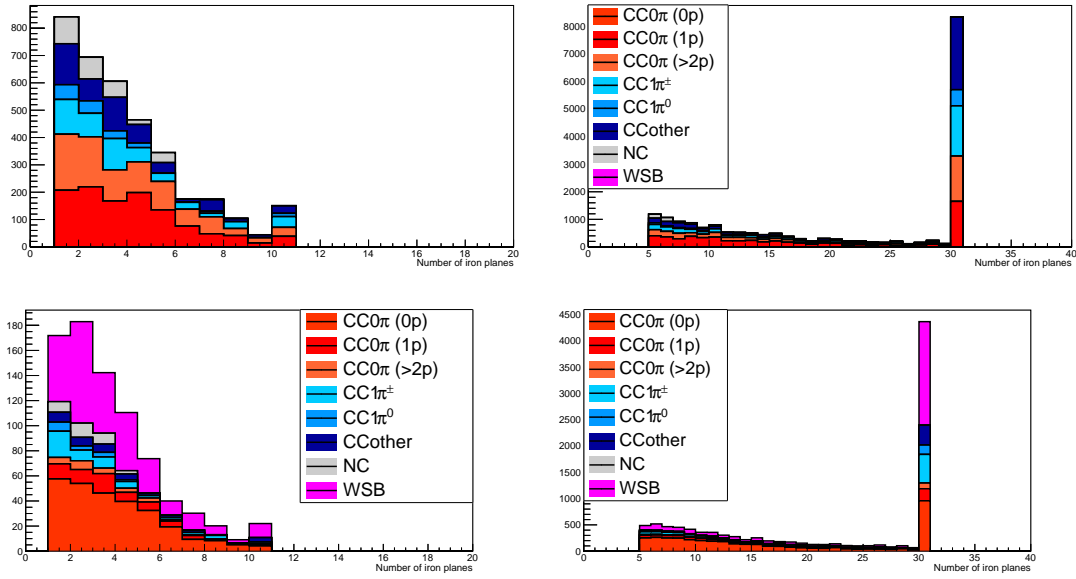


Figure 26: Iron plane numbers in Side-MRD (left) and Baby-MIND (right) corresponding to the end points of the longest tracks in the selected events in the neutrino-mode (top) and the antineutrino-mode (bottom).

546 This study is based on an original study done for the ND280 upgrade target, with some  
 547 modifications. Though the cell size is similar to the WAGASCI configuration presented  
 548 in Section 5, the external dimensions are different (1864 mm  $\times$  600 mm  $\times$  1300 mm).  
 549 Whenever the results are presented with this external size and this parameter is likely to  
 550 impact the result, it will be mentioned.

551 Note that in this section, a simplified reconstruction algorithm presented in Section 6.1 is  
 552 used. The fiducial volume is chosen accordingly as the inner cube of the module which  
 553 surfaces are  $4 \times$  scintillator space = 100 mm distant from the module external surfaces.  
 554 The neutrino interactions are simulated using NEUT v5.3.2. The NEUT input neutrino  
 555 flux is estimated using JnuBeam v13a and assuming the detector to be located at  $1.5^\circ$   
 556 off-axis, as in Section 5. Note that the event reconstruction efficiency as a function of true  
 557 neutrino energy might be changed at  $1.5^\circ$ , due for example to different  $Q^2$  distributions.  
 558 For this reason, one has to note that the reconstruction results might change slightly from  
 559  $2.5^\circ$  and  $1.5^\circ$ . To avoid a similar change on the particle-only reconstruction efficiencies,  
 560 they will be presented as a function of variables that completely characterize the particle  
 561 kinematic state, *i.e.* its momentum and angle. Figure 28 shows the vertex distributions  
 562 of the daughter particles of neutrinos interacting one standard WAGASCI water-module.  
 563 In this section, we will show the detector reconstruction and particle identification in this

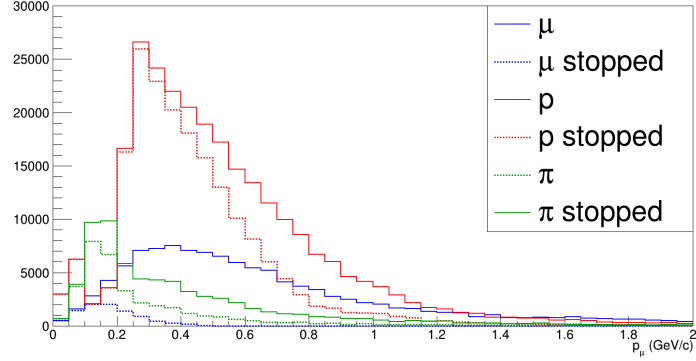


Figure 27: Momentum distribution of true particles in WAGASCI (plain) and corresponding distributions only for particles stopping into the WAGASCI module (dashed).

564 phase space, both for leptonic and hadronic particles. We will finally show an empty  
 565 WAGASCI module can highly enhance the ability to constrain the neutrino interaction  
 566 final state which is critical to reduce the corresponding uncertainties.

## 567 6.1 Reconstruction algorithm

### 568 6.1.1 Description

569 For this section, an ideal “simulated” reconstruction is developed. A particle is recon-  
 570 structed if:

- 571 1. The particle is charged.  
 572 2. Has at least one hit (energy deposit  $> 2.5$  photo-electron) in a scintillator.  
 573
- 574 3. The particle enters one TCP and has one hit in the tracker.  
 575 Or

- 576
- 577 • The particle should be long enough to be reconstructed by the detector in at  
 578 least 2 out of 3 views (XZ, YZ, XY). The length criterion requires the particle  
 579 to let at least 4 hits in the detector. In the “less favourable case” of pure  
 580 longitudinal or transverse going tracks, it represents a the track length of  $L_{track} \geq$   
 581  $4 \times$  scintillator space = 100 mm.
  - 582 • In the views where particles pass the length criterion, the particle shall not  
 583 be superimposed with longer tracks in at least two views. The superposition  
 584 criterion is estimated with the distance inter-tracks (DIT) which corresponds to

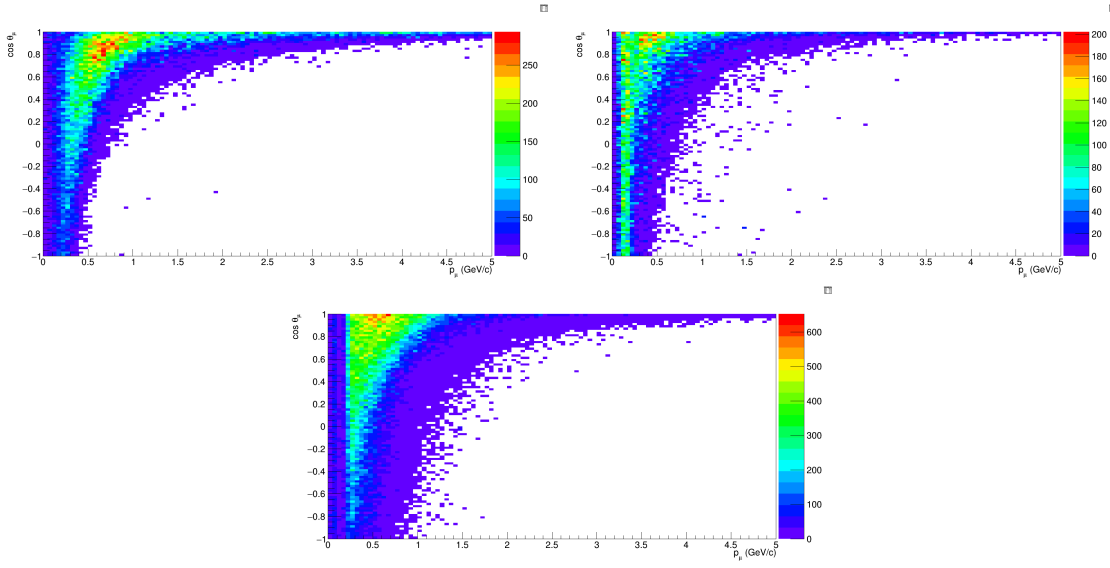


Figure 28: True number of muons (left), charged pions (right) and protons (bottom) in the two WAGASCI water-module as a function of the particles momenta and angles at  $1.5^\circ$ .

585 the orthogonal distance between two tracks at the ending point of the shortest  
 586 distance between two tracks at the ending point of the shortest one (see Figure 29). For a track we call track 1, the super position criterion is  
 587 tested with every longer track that starts at the same vertex. Let  $\vec{p}_1$  the vector  
 588 of track 1, and  $p_1^a$  its projections in the XZ, YZ and XY planes respectively for  
 589  $i=1,2,3$ . Note that these are projections onto 2D planes and not onto a direction  
 590 vector. In this case, the relative angle between track 1 and a longer track, track 2,  
 591 (of vector  $\vec{p}_2$ ) in a view a is given by:

$$\cos \theta = \frac{\vec{p}_1^a \cdot \vec{p}_2^a}{\|\vec{p}_1^a\| \|\vec{p}_2^a\|} \quad (1)$$

592 and the distance inter track is given by:

$$DIT = \|\vec{p}_1^a\| \sin \theta \quad (2)$$

593 The DIT should be higher than  $4 \times$  scintillator width for the track 1 to be not  
 594 superimposed with the track 2 in the view a, which also corresponds to 100 mm  
 595 in the nominal configuration.

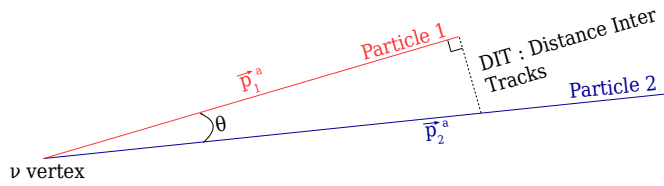


Figure 29: Definition of the distance inter tracks.

### 596 6.1.2 Performances

597 The particle-only reconstruction efficiencies and the reconstruction threshold in momenta  
 598 are shown in Table 4. This threshold is defined as the maximal momentum for which the  
 599 reconstruction efficiency is smaller than 30%. The thresholds in muon and pion momenta  
 600 are 150 MeV/c. Most of the muons are above this threshold (see Figure 28) which leads  
 601 to a 79% reconstruction efficiency.

	$\mu$	$\pi$	p
Reconstruction Efficiency	79%	52%	26%
Momentum threshold	150 MeV/c	150 MeV/c	550 MeV/c

Table 4: Reconstruction efficiency and momentum threshold for muons, pions and protons. The threshold is defined as the maximal momentum for which particles have a reconstruction efficiency smaller than 30%.

602 The lower pion and proton efficiencies (respectively 52% and 26%) are due to lower  
 603 efficiencies for similar momenta than muons, coming from strong interactions as shown  
 604 on Figures 30. Efficiencies of each particle type tend to decrease in the backward region  
 605 due to lower particle momenta. However, for a fixed momentum value, the reconstruc-  
 606 tion efficiency is almost uniform which confirms the ability of the WAGASCI detector to  
 607 reconstruct high angle tracks.

608 The reconstruction is thereafter tested on neutrino events. Table 5 summarizes the  
 609 number of reconstructed events and efficiencies for each interaction type. As expected  
 610 from the high muon reconstruction efficiency, the charged current interactions have recon-  
 611 struction efficiencies  $\geq 85\%$ .

612 The reconstruction efficiencies as a function of the neutrino energy and muon kinematics  
 613 are respectively shown on Figure 31 and 32.

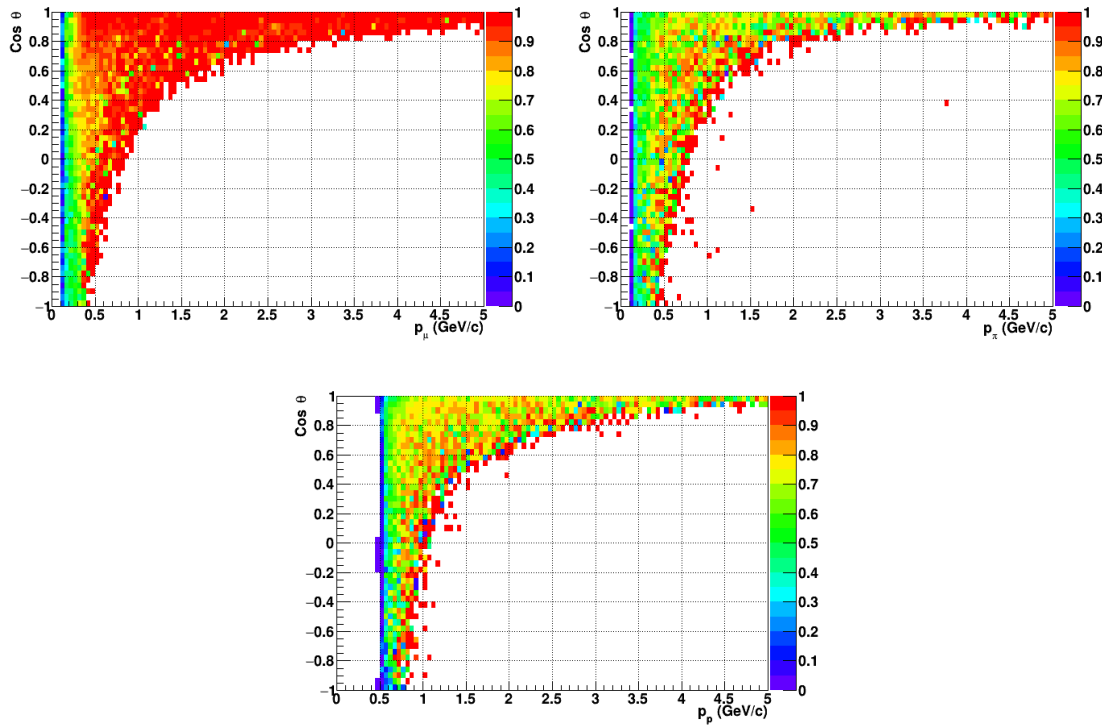


Figure 30: Reconstruction efficiency of muons (left), charged pions (right) and protons (bottom) in the WAGASCI water-module as a function of the particles momenta and angles.

	CC0 $\pi$	CC1 $\pi$	CCOthers	NC	All
Reconstruction efficiency	85%	87%	91%	22%	68%

Table 5: Number of true interactions reconstructed. The purity and reconstruction efficiency of each true interaction is also shown.

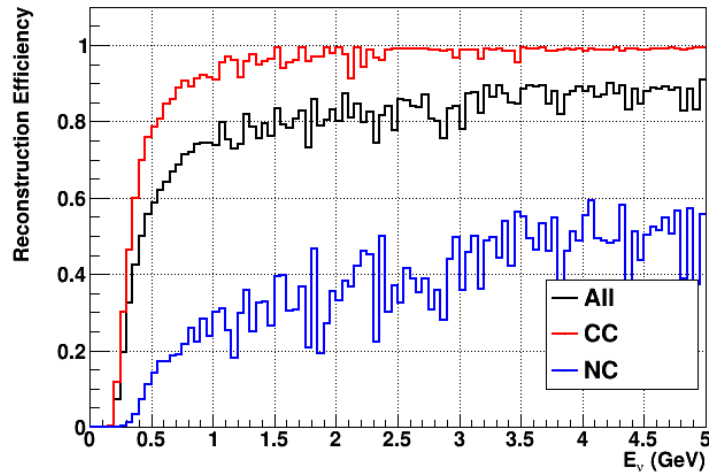


Figure 31: Reconstruction efficiency of all neutrino (black), CC (red) and NC (blue) interactions in the WAGASCI water-module as a function of the neutrino energy.

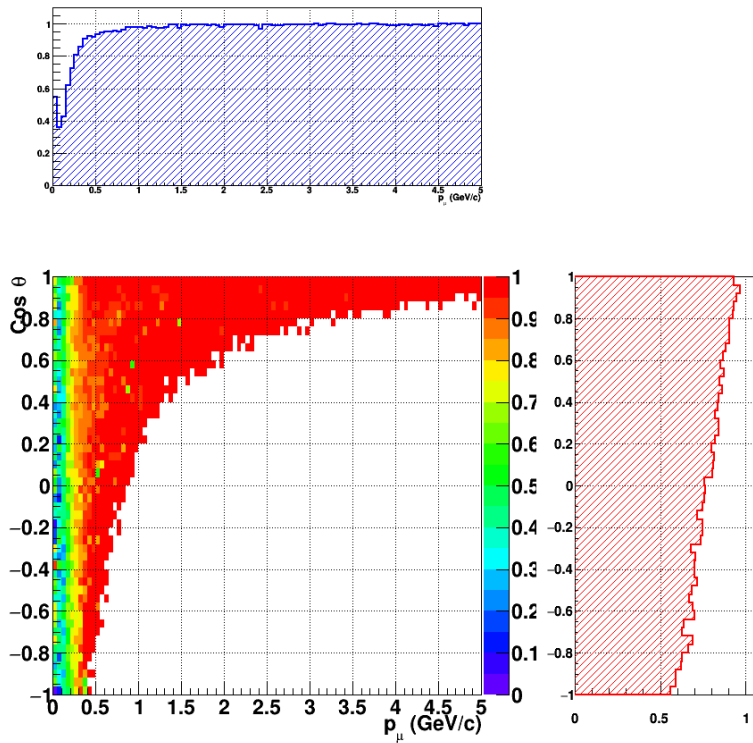


Figure 32: Reconstruction efficiency of CC interactions in the WAGASCI water-module as a function of the muon kinematic variables (momentum and angle).

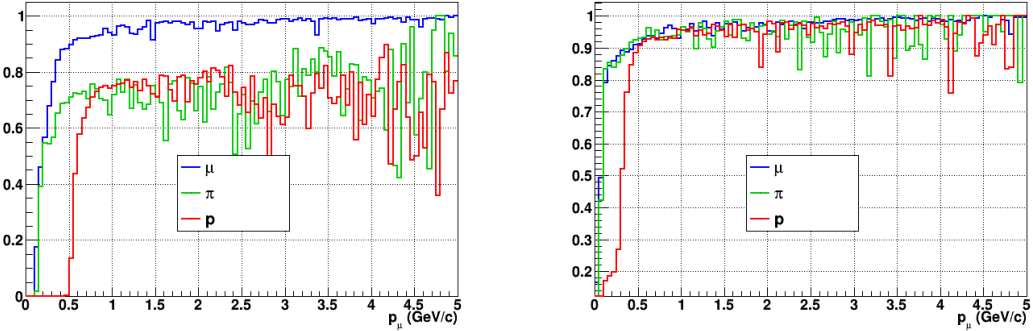


Figure 33: Reconstruction efficiency for muons, pions and protons in the water-in (left) and water-out (right) modules.

Note that a Particle Identification Algorithm has been also developed. It is based on the charge deposition of the particles in the scintillator, of the detection of a decay-electron. However, information depends highly on the number of scintillator hits by a particle, which creates an important difference between a real WAGASCI module and the one used for the ND280-upgrade simulation. For this reason, the corresponding results will not be detailed here, but can be found in [?].

## 6.2 Background subtraction: the water-out module

In the nominal configuration, 20% of the neutrino interactions occurs on scintillators ( $C_8H_8$ ). This background should be removed in order to measure the neutrino interaction on the same target as Super-K, which suppress the differences in cross-section models. For this purpose, we propose to use a water-out module, where the water is replaced by air. The detector is therefore fully active and has a 3 mm spatial resolution (scintillator thickness) which create an ideal detector to reconstruct and identify hadrons, and study np-nh interactions. The counter-part is the difference in particle energy deposition between the water and this water-out module that will need to be corrected for. In this section, we present the capabilities of such a module, and the impact it can have on cross-section measurements for the neutrino community in general and T2K in particular. The same reconstruction and selection as the water-in module is applied. Figure 33 shows the comparison between the water-in and the water-out reconstruction efficiencies for muon, pions and protons. 90% of the muons and 87% of the pions are reconstructed, while 70% of the protons are even reconstructed. It allows to lower down the proton threshold to 250 MeV/c (see Table 6).

As a consequence of tracking even low momenta particle, the reconstruction efficiency is uniform and almost maximal on the entire  $\cos \theta_\mu$  phase space, as shown on Figure 34.

	$\mu$	$\pi$	p
Reconstruction Efficiency Momentum threshold	90% 50 MeV/c	87% 50 MeV/c	70% 250 MeV/c

Table 6: Reconstruction efficiency, proportions of  $\mu$ -like and non  $\mu$ -like and momentum threshold for muons, pions and protons in the empty module. The threshold is defined as the maximal momentum for which particles have a reconstruction efficiency smaller than 20%.

638 Since the fiducial mass represents 0.25 tons, the total number of events is divided by a  
 639 factor of 3 compared to the water-in module. The water-out module offers interesting  
 640 possibilities to study np-nh interaction since 70% of the protons are reconstructed. In the  
 641 future, a possible separation as a function of the number of proton track will be studied.  
 642 Moreover, we are currently pursuing the use of single and double transverse variables (cite  
 643 Xianguo) to open new possibilities for separating np-nh from Final State Interactions, or  
 644 for isolating the interactions on hydrogen from interactions on carbon in this module.

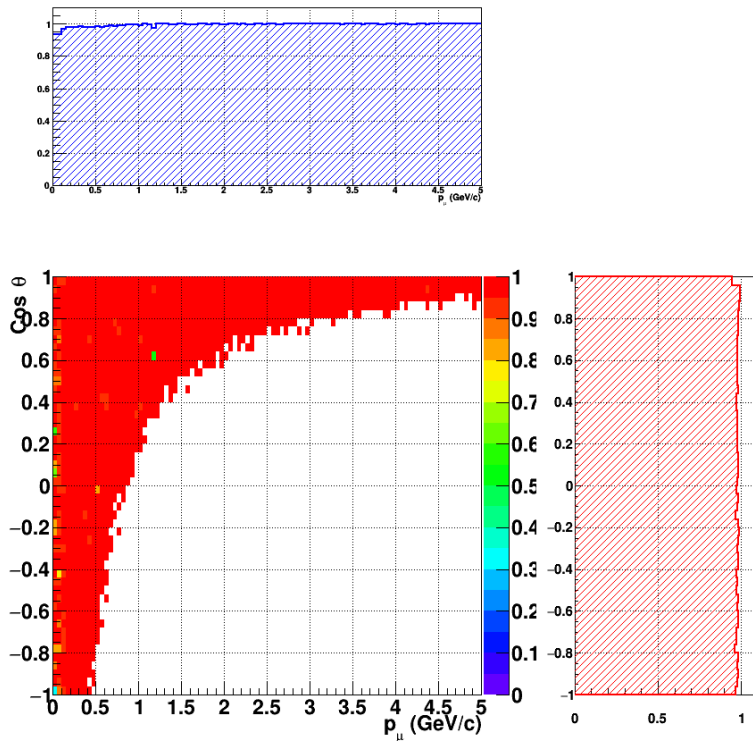


Figure 34: Reconstruction efficiency of CC interactions in the WAGASCI empty module as a function of the muon kinematic variables (momentum and angle).

645 **7 Schedule**

646 We would like to start a physics data taking from T2K beam time after the summer  
647 shutdown in 2018. By then, commissioning and tests of the detectors will be completed  
648 in J-PARC T59. The experiment can run parasitically with T2K, therefore we request no  
649 dedicated beam time nor beam condition as discussed in the following section.

650 Once the approved POT is accumulated, the WAGASCI modules will be removed  
651 from the experimental site, but we would like to keep the Baby-MIND and the Side-MRD  
652 modules on the B2 floor of the NM pit as common platforms of future neutrino experiments  
653 using the T2K neutrino beam.

654 **8 Requests**

655 **8.1 Neutrino beam**

656 The experiment can run parasitically with T2K, therefore we request no dedicated beam  
657 time nor beam condition. As data taking periods, we request the ‘nominal’ T2K one-year  
658 operation both for the neutrino beam and the antineutrino beam. The T2K has been  
659 requesting  $0.9 \times 10^{21}$  POT/year and actually accumulating about  $0.7 \times 10^{21}$  POT/year in  
660 recent years. For each year, starting from the Autumn, T2K is running predominantly in  
661 the neutrino mode or in the antineutrino mode. Our request is to have one-year neutrino-  
662 mode data and another one-year antineutrino mode data assuming that the POT for the  
663 fast extraction in each year is more than  $0.5 \times 10^{21}$  POT.

664 **8.2 Equipment request including power line**

665 We request the followings in terms of equipment on the B2 floor:

- 666 • Site for the WAGASCI modules, Side-MRD modules and BabyMIND and their elec-  
667 tronics system on the B2 floor of the near detector hall (Figure 2 and 3).
- 668 • Anchor points (holes) on the B2 floor to secure the WAGASCI modules, Side-MRD  
669 module and Baby-MIND, detailed floor plans to be communicated in a separate  
670 document.
- 671 • Power line for the magnets in Baby-MIND: 400 V tri-phase 48-to-62 Hz, capable of  
672 delivering 12 kW. We have a wish for the magnet power line to be installed and  
673 available to us by beginning of March 2018.
- 674 • Electricity for electronics and water circulation system, 3 kW, standard Japanese  
675 electrical sockets.

- 676 1. Online PCs: 2.1 kW

677            2. Electronics: 0.7 kW

678            3. Water sensors: 1 kW

- 679        • Air conditioner for cooling heat generation at Baby-MIND magnets, online PCs and  
680            electeronics
- 681        • Beam timing signal and spill information
- 682        • Network connection

683        The infrastructure for much of the above exists already. Exceptions are the power line  
684        for the magnet and the electronics and holes in the B2 floor to anchor the detector support  
685        structures.

## 686        References

- 687 [1] K. Abe et al. Measurement of the muon neutrino inclusive charged-current cross  
688        section in the energy range of 13 GeV with the T2K INGRID detector. *Phys. Rev.*,  
689        D93(7):072002, 2016.
- 690 [2] K. Abe et al. Measurement of neutrino and antineutrino oscillations by the T2K  
691        experiment including a new additional sample of  $\nu_e$  interactions at the far detector.  
692        *Phys. Rev.*, D96(9):092006, 2017.
- 693 [3] M. Antonova et al. Baby MIND Experiment Construction Status. In *Prospects in*  
694        *Neutrino Physics (NuPhys2016) London, London, United Kingdom, December 12-14,*  
695        2016, 2017.
- 696 [4] K. Nitta et al. The k2k scibar detector. *Nucl. Instrum. Meth. A*, 535:147, 2004.
- 697 [5] K. Abe et al. (T2K Collaboration). Measurement of the inclusive  $\nu_\mu$  charged current  
698        cross section on iron and hydrocarbon in the t2k on-axis neutrino beam. *Phys. Rev.*  
699        D, 90:052010, 2014.
- 700 [6] F. Magniette F. Gastaldi, R. Cornat and V. Boudry. A scalable gigabit data acquisition  
701        system for calorimeters for linear collider. *proceedings of TIPP2014*, page PoS 193,  
702        2014.
- 703 [7] J. Fleury, S. Callier, C. de La Taille, N. Seguin, D. Thienpont, F. Dulucq, S. Ahmad,  
704        and G. Martin. Petiroc and Citiroc: front-end ASICs for SiPM read-out and ToF  
705        applications. *JINST*, 9:C01049, 2014.
- 706 [8] M. B. Barbaro J. A. Caballero T. W. Donnelly G. D. Megias, J. E. Amaro. Inclusive  
707        electron scattering within the susav2 meson-exchange current approach. *Phys. Rev.*  
708        D, 94:013012, 2016.

- 709 [9] M. Valverde J. Nieves, J. E. Amaro. Inclusive quasi-elastic neutrino reactions. *Phys.*  
710 *Rev. C*, 70:055503, 2004.
- 711 [10] Yu. G. Kudenko, L. S. Littenberg, V. A. Mayatsky, O. V. Mineev, and N. V. Ershov.  
712 Extruded plastic counters with WLS fiber readout. *Nucl. Instrum. Meth.*, A469:340–  
713 346, 2001.
- 714 [11] O. Mineev, Yu. Kudenko, Yu. Musienko, I. Polyansky, and N. Yershov. Scintillator  
715 detectors with long WLS fibers and multi-pixel photodiodes. *JINST*, 6:P12004, 2011.
- 716 [12] Etam Noah et al. Readout scheme for the Baby-MIND detector. *PoS*, Pho-  
717 toDet2015:031, 2016.
- 718 [13] Omega. Spiroc 2 user guide. 2009.